Image-Based Approaches to Hair Modeling

Dissertation

zur

Erlangung des Doktorgrades (Dr. rer. nat)

der

Mathematisch-Naturwissenschaftlichen Fakultät

der

Rheinischen Friedrich-Wilhelms-Universität Bonn

vorgelegt von

Tomás Lay Herrera

aus

Havanna

Bonn, November 2012

Gedruckt mit Unterstützung des Deutschen Akademischen Austauchdienstes.

Angefertigt mit Genehmigung der Mathematisch-Naturwissenschaftlichen Fakultät der Rheinischen Friedrich-Wilhelms-Universität Bonn

- 1. Gutachter: Prof. Dr. Andreas Weber
- 2. Gutachter: Prof. Dr. Thomas Vetter
- Tag der Promotion: 12. April 2013
- Erscheinungsjahr: 2013

... a mi abuela Martha, que siempre creyó que yo iba a “llegar lejos”, y a Rosa, que ha llegado conmigo hasta aquí.

Acknowledgment

Ante todo quiero agradecerle a Rosa, por estar siempre ahí. También a los viejos, por ayudarme a ser como soy. A mis tíos, tías y primos, por todo el cariño que me han dado. A Doris, por su ayuda. A Alejandro Mesejo y Angela León, por la Numérica y los Sistemas de Partículas. Al Samu, Erddys, Mario, Javier, Nesti, Mijail, Luiso, Batista y a todos mis compañeros de "carrera". A Angie, Patrick y Emilia, Diana y Alejo, Juanita, Felipe y Jacobo, Fernando y demás "Alma-Marcelianos", por las risas y las alegrías.

Sin ustedes no hubiese sido posible.

Bedanken möchte ich mich zuallererst bei Andreas Weber für sein ständiges Vertrauen und seine Unterstützung. Auch bei Arno Zinke – ohne ihn wäre mein Weg viel länger gewesen.

Darüber hinaus gilt mein Dank meinen Kollegen Björn Krüger, Jan Bauman, Jochen Tautges und Hassan Errami für ihre Hilfe und die gute Zusammenarbeit; Thomas Vetter, Pascal Paysan und Brian Amberg für die Kopfmodelle und die Gesichtstexturen; Bernd Brüggeman und Michael Kortmann für die Wärmebildkamera; Alejandro, Anna, Janne, Rita, Felipe, Rosa Maria und Angela für die wertvolle Hilfe mit den Frisuren; Susanne Röhrig für jene E-mail mit der alles anfing. Insbesondere bedanke ich mich beim DAAD, der diese Arbeit ermöglichte.

Ein weiteres herzliches Dankeschön geht an meine Bonner Freunde, insbesondere Giovanni, die Lenzens, die Rudertruppe und den Rhein für das schöne Zusammenleben und das unschätzbare Zuhausegefühl.

Ohne Euch wäre es gar nicht möglich gewesen.

Abstract

Hair is a relevant characteristic of virtual characters, therefore the modeling of plausible facial hair and hairstyles is an essential step in the generation of computer generated (CG) avatars. However, the inherent geometric complexity of hair together with the huge number of filaments of an average human head make the task of modeling hairstyles a very challenging one. To date this is commonly a manual process which requires artist skills or very specialized and costly acquisition software.

In this work we present an image-based approach to model facial hair (beard and eyebrows) and (head) hairstyles. Since facial hair is usually much shorter than the average head hair two different methods are presented, adapted to the characteristics of the hair to be modeled. Facial hair is modeled using data extracted from facial texture images and missing information is inferred by means of a database-driven prior model. Our hairstyle reconstruction technique employs images of the hair to be modeled taken with a thermal camera. The major advantage of our thermal image-based method over conventional image-based techniques lies on the fact that during data capture the hairstyle is "lit from the inside": the thermal camera captures heat irradiated by the head and actively re-emitted by the hair filaments almost isotropically. Following this approach we can avoid several issues of conventional image-based techniques, like shadowing or anisotropy in reflectance.

The presented technique requires minimal user interaction and a simple acquisition setup. Several challenging examples demonstrate the potential of the proposed approach.

Contents

1

Introduction

Over the last years we have seen how the computing power of graphic workstations have increased considerably. These improvements in hardware have made possible the generation of every time more realistic computer-generated (CG) environments to the point that sometimes is really hard to discern whether a displayed content is computer generated or not. Because of the influence of hair in the overall appearance of virtual avatars, hair modeling plays a very relevant role during generation of computer-generated (CG) humans.

Hair modeling is, nevertheless, a very challenging task. During our life we see thousands of different real hairstyles and our brain can recognize them quite well, hence "fooling" it with CG hair is not that easy. On the other hand, a typical hairstyle has over 100000 filaments, long and thin structures with complicated photometric and geometric properties. Moreover, the complex way the filaments interact with each other and with the exterior environment has a direct impact in the hairstyle's final appearance and makes

the modeling task even more difficult. Therefore the development of efficient approaches to model human hair is still necessary, despite the advances in graphic hardware.

In this work an approach for modeling facial hair (beards and eyebrows) and (head) hairstyles is presented. Our approach is image-based, meaning that the resultant hair geometry is generated using as input information collected from images. Following this approach the user interaction in the modeling pipeline is minimized and the results can be directly validated against the input data. The information required to model facial hair is extracted from facial texture images [PKA+09] (Figure 1.1) and improved with a database-driven prior model. The output of this approach is a set of hair filaments, represented by interconnected rigid segments, reproducing the modeled facial hair.

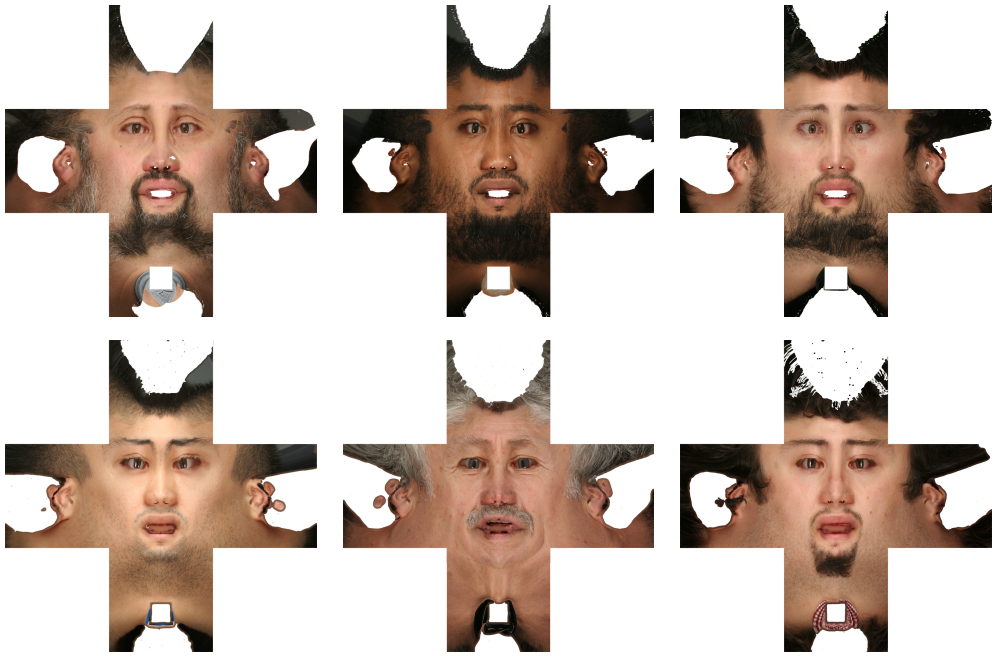

Figure 1.1: Facial texture images used as input in our facial hair generation technique.

The input of the hairstyle modeling pipeline is a set of images taken with a thermographic camera. A thermographic –or infrared– camera is a capturing

device that detects radiation in the infrared range of the electromagnetic spectrum (0.75 µm–14 µm) and forms an image –also called thermogram– from that radiation. Using a thermographic camera we are able to measure the heat –in form of electromagnetic radiation– emitted by the human head and actively re-emitted in a diffuse way by the hair filaments, thus bypassing common problems of conventional image-based reconstruction approaches, like shadowing or directional highlights (Figure 1.2). The resultant hair geometry is represented by a set of geometric curves resembling the shape of the reconstructed filaments.

Figure 1.2: Comparison between conventional and thermal, color coded images.

1.1 Properties of Human Hair

Hair is a filamentous appendage that grows from large cavities called follicles located in the dermis. It is primarily composed of protein, mainly keratin, and grows in humans over a large percentage of the body surface. Hair is characteristic of all mammals and provides protective, sensory and sexual attractiveness function.

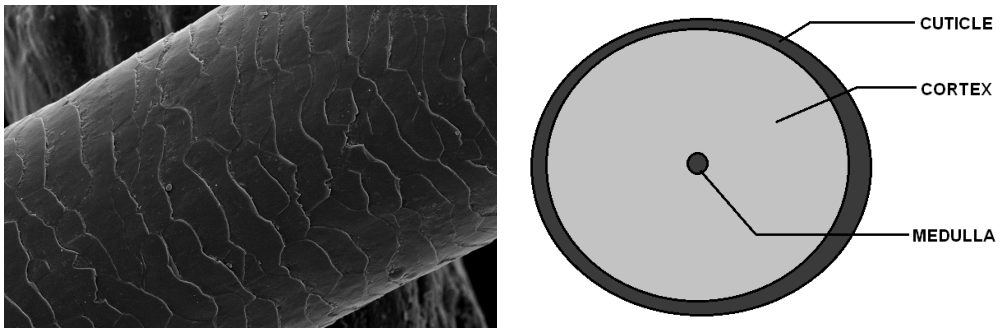

Figure 1.3: Left: Hair filament seen through a scanning electron microscope. Source: University College Cork, Ireland. Right: Cross section of a hair fiber.

Hair filaments are composed of three concentric structures (Figure 1.3). The outermost layer is the **cuticle**, a thick protective covering made up of 6 to 8 layers of flat overlapping structures like tiles on a roof. The cuticle surround the **cortex**, which accounts for 90% of the filament's weight. This structure is responsible for the physical properties –shape, curliness, elasticty– of hair. Moreover, cortical cells contains melanin, the pigment responsible for the color of the hair. Surrounded by the cortex and located near the center of the fiber is the **medulla**, composed by loosely connected keratinized cells. The diameter of human hair filaments varies from 50 µm to 100 µm.

Regardless of location, hair fibers grow in a cyclical manner consisting in three distinct phases: *anagen phase* (growing stage) which lasts from two to six years, *catagen phase* (transition stage) lasting only 1-2 weeks and *telogen phase* (resting stage) which lasts for 5 to 6 weeks [Rob02]. The shape of the follicle where the filament grows determines the shape of the cortex, and the shape of the cortex is related to the curliness of the hair fiber. Straight filaments have a rather round cross section whereas wavy or curly hair have generally an oval or irregular cross section. According to its degree of curliness (or curl pattern), hair can be classified as straight, wavy, curly or kinky (Figure 1.4).

Figure 1.4: Hairstyles with different degree of curliness. From left to right, top to bottom: straight, wavy, curly and kinky hair.

1.2 Related Work

1.2.1 Image-Based Modeling

Three-dimensional (3D) reconstruction is an area in computer graphics and computer vision that deals with the computation of shape and appearance of

real world objects. Approaches for 3D reconstruction usually rely on physical techniques like laser scanners or structured light to collect data and generate a usable geometrical model [BR02, GAVN11, FE08, PKA+09]. Although quite accurate, such reconstruction techniques have limitations: color information must be provided by an extra capturing device. Moreover, such devices cannot capture the shape of hair due to its reflection properties.

Image-based Modelling is a passive 3D modelling approach in which the object's shape is reconstructed using information extracted from multiple images [HZ04]. An image is essentially the projection of a 3D scene onto a 2D plane and during reconstruction the the spatial location of all objects in the scene is computed. This computation is accomplished in such a way that the projection of the reconstructed objects conforms with the original images.

1.2.2 Thermal Imaging

According to the *Black Body Radiation Law* all objects with temperature above absolute zero emit infrared radiation. The amount of radiation emitted by a body increases with its temperature, therefore thermal cameras can be used to detect temperature variations. Moreover, thermograms can depict a scene without illumination, since the measured radiation comes from the captured objects. Due to these properties, thermal imaging is used in several fields, going from military or surveillance to building inspection, medicine or process monitoring [Bro12, Rob12, Mer12, AKN+11].

In computer vision several thermography-based approaches have been proposed recently: Cardone et al. [CIIP12] propose a methodology to accurately project temperature maps on 3D objects. The technique proposed by Filipe and Alexandre [Fil10] performs an automatic segmentation of thermal face images. Bilodeau et al. [BTL+11] present an approach to measure the temperature of moving objects in a non-invasive way using thermographs. Yang and Chen [YC11] propose a method to obtain the 3D surface temperature distribution of an object using a thermal imaging system based on structured light. In an attempt to speed up existing building inspection

techniques, Lagüela et al. [LAGJ+12] presented a relative simple and interactive procedure to fuse visual and thermal images of buildings. Luhmann et al. [LOPR10] presents an overview of different thermal image sensors and proposes a technique for the geometric calibration of thermographic cameras. Stennett and Harris [SH] analyse the performance of two conventional image-based 3D computer vision systems when using thermal data.

1.2.3 Hair Modeling

Since the pioneering work presented by Anjyo et al. [AUK92] modeled hair filaments as cantilever beams many other approaches have been developed to generate plausible hairstyles. Simulating each hair filament independently can be very complicated and time-consuming. Fortunately, adjacent hair strands tend to form wisps and behave in a similar way [WS92]. Considering that, hairstyles have been modeled by wisp models [CK05], characterizing each wisp by a guide strand. The wisp information has been coded in surfaces [KN00], has been arranged in multi-resolution models in which a hierarchy of generalized cylinders is implemented [KN02] or in a level-of-detail model that includes individual strands, hair clusters and hair strips representing the whole hairstyle [WLL+03]. All these techniques require considerable manual work, therefore the generation of a plausible hairstyle requires both time and skills from the user: a good example is "Hair Meshes", an interactive tool presented by Yuksel et al. [YSK09].

Other approaches predict the shape of hair filaments based on physical models. Among the contributions to this sub-area are the works of Hadap and Magnenat-Thalmann [HMT00] in which the hair filaments are modeled as streamlines of a fluid flow, or Bando et al. [BCN03] where the hairstyle is characterized using particles sampled within the hair volume. Bertails et al. [BAQ+05] propose a mechanical model based on the Cosserat equations while the approach of Sobottka et al. [SKW06] generate hairstyles by fitting the hair geometry into a hair volume obtained from surface scans.

Image-based approaches attempt to reconstruct a hairstyle based on information extracted from different views of a hair model. These techniques

neither require major user interaction nor involve the simulation of extremely complex physical models. Grabli et al. [GSML02] estimated the orientation of hair strands by analysis of the hair model under varying illumination and Paris et al. [PBnS04] improved this approach by capturing the model from 4 fixed viewpoints, being thus able to compute a 3D orientation vector field of the whole hairstyle. The work of Wei et al. [WOQS05] was the first attempt to reconstruct a hairstyle in out-of-lab conditions, employing only a hand-held camera. Using a hand-held camera and available light simplifies considerably the acquisition setup, however lot of information of the hair model gets lost, since the computed orientation information is projected on the model's visual hull. Paris et al. [PCK+08] proposed a pipeline based on dome-like capture setup, consisting in 16 cameras, 150 LED light sources and 3 DLP projectors. Although the proposed technique is able to reconstruct a hairstyle down to the filament level, the extremely complex acquisition setup represents a major drawback. Another approach to model hair fibers, however only suitable for small hair tresses, was presented by Jakob et al. [JMM09]. The input of this technique are macro photographs of the hair wisp taken with a very shallow depth of field, allowing to isolate the hair filaments.

1.3 Structure of the document

The remainder of this work is organized as follows: In Chapter 2 we describe our facial hair modeling technique, introducing our color-and-frequency-based hair region segmentation algorithm. We also show how we infer missing data based on statistical models derived from a database of facial texture images. Chapter 3 describes our thermal-based approach for hairstyle reconstruction, showing how the issues related to the use of conventional images are avoided by the use of thermograms. Finally we close the thesis with conclusions and some proposals for future research.

2

Facial Hair Modeling

The approach presented in this chapter models facial hair –beards and eyebrows– using information extracted from facial texture images. A prior model built upon a database of facial hair distributions helps to improve the quality of the synthesized hair geometry in cases where the information extracted from the input data is not accurate enough.

2.1 Introduction

The presence of plausible facial hair brings lot of realism to virtual avatars. Due to its important role in the creation of CG-generated characters and its high degree of complexity, hair simulation has been analyzed several times from different perspectives [WBK+07, HCL+07, BHC+08, BBN+12]. Despite being closely related to the more researched field of hairstyle modeling, facial hair modeling has not received much attention. Although at first glance seems to be relatively simple –specially if compared with hairstyle modeling–

the automatic image-based modeling of beards and eyebrows is a very challenging task, as all information required for facial hair synthesis has to be automatically extracted from the texture images.

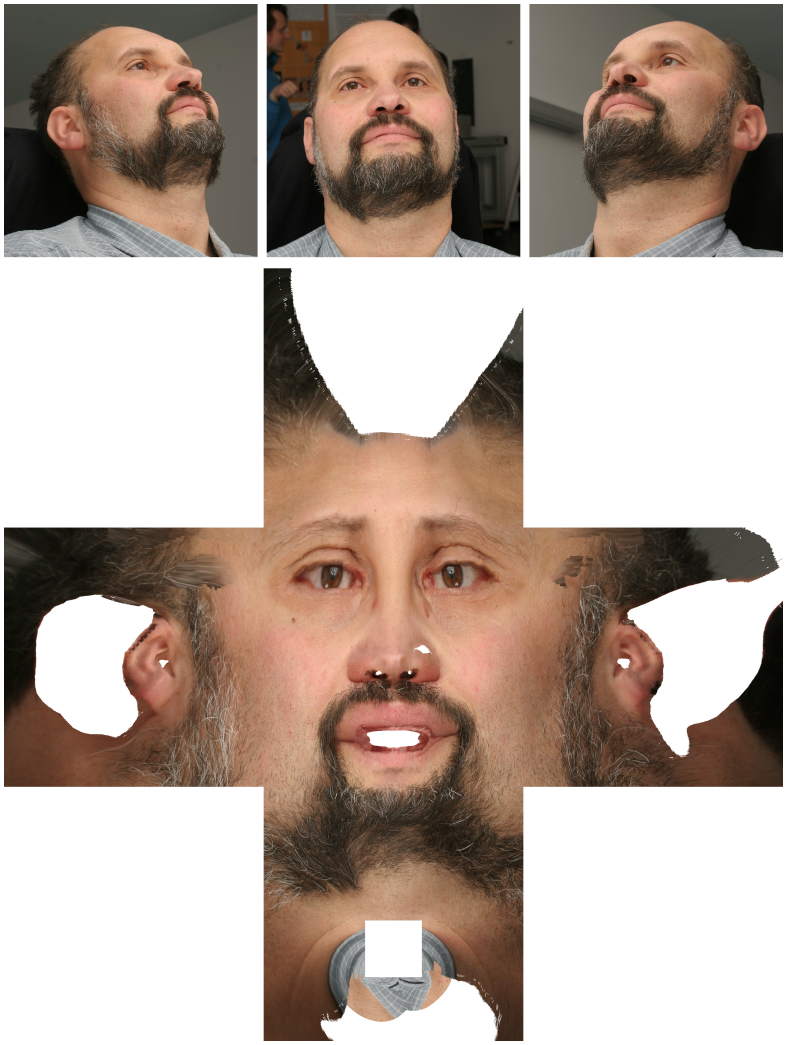

Figure 2.1: Top row: Sequence of images used for the generation of the facial texture. Bottom image: Generated facial texture following the approach presented in [PKA+09].

Facial hair has, however, a major advantage over hairstyles: facial hair filaments are typically shorter –and hence easier to model– than hairstyle filaments and usually grow forming a layer parallel to the face. Moreover, as they are not stylized, facial hair has a predominant direction without

complicated orientation patterns that often appear in hairstyles. Based on that, the problem of modeling facial hair can be reduced to the localization of the hair regions on the texture images and the computation of the local image orientation in those regions.

Since the input data of our approach consists of registered texture images and their corresponding head models (Figure 2.2), the information characterizing the facial hair is transferred from the images to the models following a one-to-one correspondence between the texture and model coordinates. Another advantage of our approach is that, since we have the head mesh, we do not have to infer the position of the chin or other regions occluded by the facial hair.

2.1.1 Overview

Our pipeline has two stages: "feature analysis" and "geometry synthesis" (Figure 2.2). In the "feature analysis" stage features are extracted pixel-wise from the texture image of the input model S using image processing techniques. These features will help us to estimate the location of hair in the image, together with its corresponding 2D orientation. This stage is also applied to a database of texture images from different individuals –as a pre-processing step– to estimate a statistical prior representing the a-priory likelihood of hair distribution in the texture images. The prior information is used to improve the results of the "feature analysis" step in case that the input information is missing or unreliable.

During "geometry synthesis" the extracted features are transferred from the texture image space to the head model space and used to synthesize hair geometry on the target head model T. The texture images are registered with the head models, meaning that we have a bijection between the two-dimensional image space and the three-dimensional model space. This one-to-one correspondence is key in this step, allowing a simple mapping of the features. The facial hair geometry is generated as a group of connected 3-D filaments employing a "particle shooting" method.

The main contributions of the presented approach are

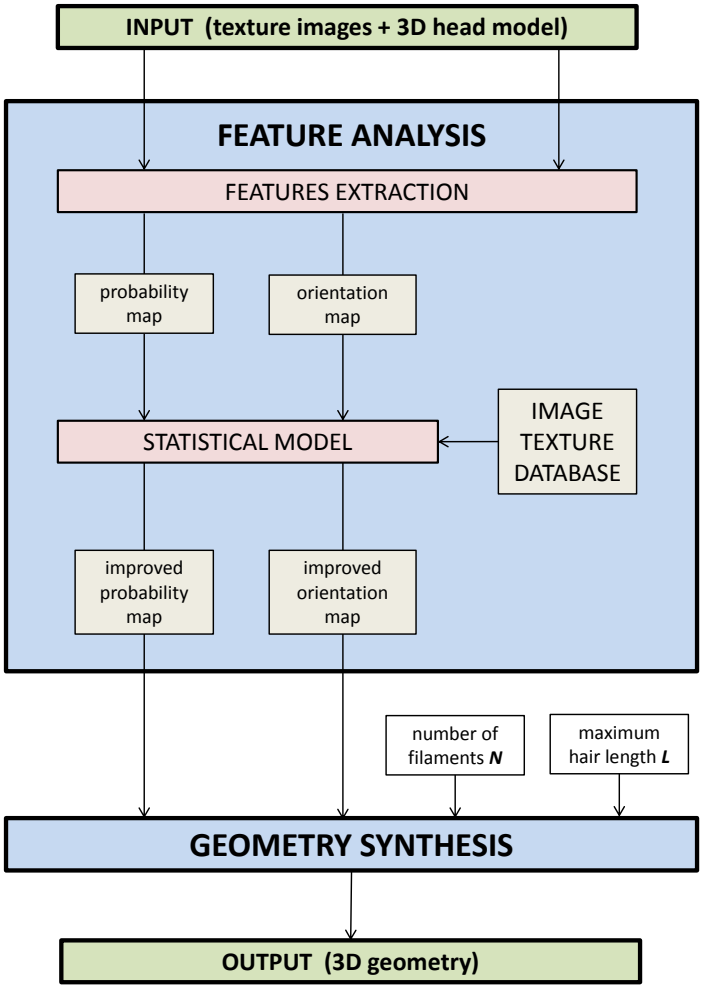

Figure 2.2: Workflow of the facial hair transfer process.

- A novel measure estimating the probability of a pixel to belong to either skin or hair. This measure is inferred from statistics of the texture image of a source model S. The new approach works fully automated and is robust with respect to color tone variations of both skin and hair.

- A method for estimating 2D strand orientation as well as hair density in texture space.

- A statistical prior based on features of over 70 individuals that im-

proves the plausibility of results even in difficult cases with missing or incomplete texture information.

2.1.2 Related Work

As already mentioned, facial hair is characterized by its location and local orientation in the texture images. Therefore the quality of our results is closely related to the accuracy of the segmented hair region, the extracted image orientation and estimated hair length.

Hair-Skin Segmentation The extraction of the hair regions on the input images account for the most important part of the problem to solve, since all information required to synthesize a plausible facial hair geometry is extracted from those regions. Due to its relevance, detection of hair and skin regions on facial images has been discussed several times from different viewpoints, as solutions to this problem play a fundamental role in a wide range of applications that go from face detection and gesture analysis to human computer interaction.

The partitioning of the input images into hair and skin regions can be seen as a typical segmentation problem. By modeling an image as a piecewise smooth function, the segmentation problem consist in computing the partition of the image domain in a set of pixels or *segments* such that the function behaves smoothly within each segment and shows discontinuities across the segment boundaries. Following this definition the segmentation of an image reduces to the computation of an optimal approximation of the original function by a set of piecewise smooth functions defined on the different segments. This optimal combination can be obtained by minimizing the *Mumford-Shah functional* [MS89]. Many different solutions have been proposed for the problem of image segmentation, going from clustering algorithms [Llo06] to graph cut-based techniques [BV06] or level set methods [MSV95].

The majority of hair and skin detection techniques on images are based on color information and the two main problems to solve are the selection of a suitable color space and the modeling of the skin color distribution. Among

the most widely proposed color spaces are the **RGB** –the most commonly used format to represent color information– and its normalized version **rgb**. Perceptual color spaces like **HSI** or **HSL**, where color is expressed as a combination of hue (**H**), saturation (**S**) and intensity (**I**), are also frequently used. Perceptually uniform color spaces, such as **CIELab** or **CIELuv**, have the convenient property that perceptive differences between two colors are equally reflected in the color representation [Poy97], but nonlinear transforms involved in the conversion to and from **RGB** represent a drawback.

The distribution of the of the skin (hair) color can be specified **explicitly** be means of constraints [KPS03] or modeled using parametric or nonparametric models. In parametric models, like **Gaussian classifiers** or **elliptical boundary models**, the color distribution used to compute the probability for a pixel to belong to the skin (hair) region is modeled explicitly, whereas in nonparametric models, such as **histogram models** or **Bayes classifiers**, the probability is estimated by comparing its color with color information extracted from training data.

The work presented by Phung et al. [PBC05] presents a comparative study of different color representations and classification algorithms for pixelwise skin segmentation. The algorithms are evaluated on a database of 4000 color images together with manually generated ground-truths. Gasparini and Schettini [GS06] propose a method in which a genetic algorithm is employed to explicitly specify the skin distribution in different color spaces. The performance of the algorithm is tested using a large and heterogeneous skin database [JR99]. The approach presented by Mohr and Zachmann [MZ07] detects skin regions using three dimensional Gaussians that represent the color distribution on *homogeneous regions*, detected combining color and edge information. Finally, the technique proposed by Sun [Sun10] combines color models built from training images to detect skin pixels in unknown images. These detected pixels adapt the color model to the unknown image, improving thus the segmentation results. Several comprehensive studies about color-based segmentation have been published in the last years [VSA03, KMB07, KHSB12].

Other approaches combine color with additional information to obtain an

accurate segmentation. Phung et al. [PBC03] proposes an approach in which the boundaries of potential skin regions detected using a Bayesian model are refined using edge information. Ruiz-del-Solar and Verschae [SV04] also exploit the homogeneity of the skin regions and skin is detected as the result of a diffusion process. Yacoob and Davis [YD06] assume that the faces are in frontal view and combines face recognition techniques with skin color modeling to automatically extract and characterize the hair region from images. The performance of this approach is tested on a dataset of 524 subjects and 3100 images of the AR dataset [MB98]. Rousset and Coulon [RC08] propose a method to extract the hair mask detecting automatically the head region in the image and analysing the color and frequency information around it. The results are evaluated by comparing them with semi-manually segmented images. Lee et al. [LASG08] propose a probabilistic hair and face segmentation algorithm that uses a Gaussian Mixture Model (GMM) combining color and position information of face and hair regions.

Local Image Orientation Over the last years several approaches that estimate the local orientation of an image have been presented. Freeman and Adelson [FA91] presented the "steerable filter", a class of filters synthesized as a linear combination of "basis filters" that can be "steered" to any arbitrary direction and the maximum of its response as a function of the angle denotes the predominant orientation. Several basis sets as well as their corresponding Hilbert transforms can be found in [FA91]. However, this kind of filters suffer from π-periodicity, as the directional derivatives of Gaussians used to synthesize them are symmetric or antisymmetric. To avoid this issue Simoncelli and Farid [SF96] proposed a new class of asymmetric steerable filters.

Feng and Milanfar [FM02] presented an approach in which local orientation is estimated using Principal Component Analysis (PCA) in a multi-scale fashion to improve its robustness to noise. Local image orientation can be also be estimated using structure tensors. Structure tensors –also called second moment matrices– are matrices whose eigenvalues and eigenvectors describe the local orientation of the image, therefore perfectly suited for tasks

involving orientation analysis. Brox et al. [BWBM06] proposes a nonlinear variation of structure tensors that can be used to estimate image orientation, whereas Kothe [Kot03] presented the *boundary tensors*, also a variation of the structure tensors.

We follow the approach proposed by Freeman and Adelson [FA91] and compute the local orientation in the hair regions using "steerable filters".

2.2 Feature Analysis

Figure 2.3: Example of facial texture image from an input model.

In order to successfully characterize the facial hair on the input model S, we need to know the location of hair on the face and the direction in which it grows. To obtain this information we find the "hair regions" on the the texture images and then calculate the 2D image orientation on them.

Since all the subsequent steps depend on an accurate extraction of the hair regions, an efficient and robust technique to detect them on the texture images is indispensable. This technique should also be able to overcome issues like unbalanced illumination –causing shadows or highlights– and has to be invariant to different skin and hair colors.

For our estimation purposes, we distinguish two regions: a hair region and a skin region, where every pixel in the image belongs either to the former or to the latter. The type of images we are working with (Figure 2.3), where no background or other distracting elements are present, makes this assumption possible. Following this idealized consideration we then calculate for every texel $t_{(i,j)}$ the probability $p_{\text{hair}}^{(i,j)}$ that it belongs to the hair region. The resulting probability chart characterizes the facial hair distribution that we are looking for.

2.2.1 Discriminating Skin and Hair –Feature Set

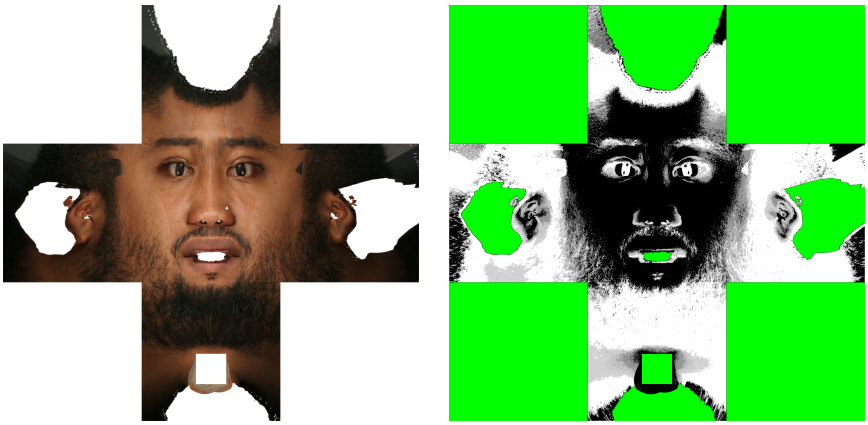

Figure 2.4: Purely color-based segmentation techniques fail if hair and skin have similar tonality.

Color is the simplest and most intuitive way to check whether a texel belongs to the hair or to the skin region. The downside of this approach is that techniques based solely on the texel's color lack of robustness, due to the drastic effect that disturbing illumination effects like shadowing and highlights have on a texel's tonality [KMB07]. Moreover, purely color-based

segmentation techniques fail in cases where skin and hair have rather similar colors (Figure 2.4). Therefore, to improve the robustness of the segmentation not only color but other features have to be taken in to consideration.

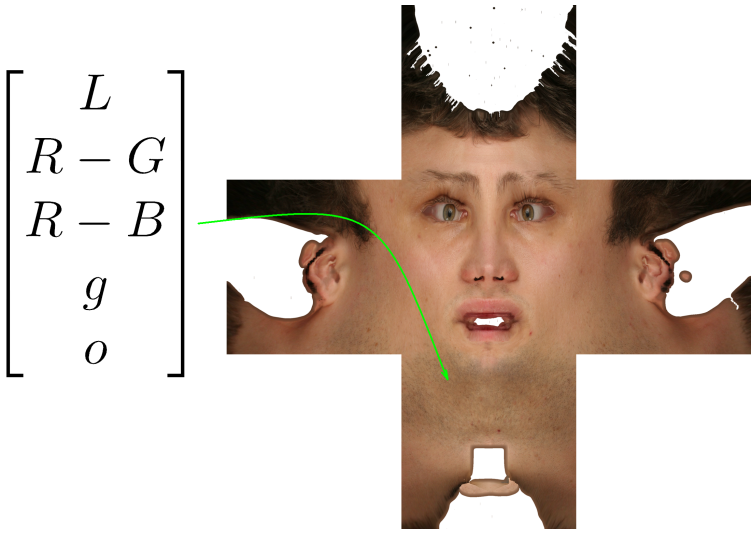

Figure 2.5: Feature vector calculated on a texel basis.

To overcome this issue, our method is based on a feature vector calculated for each texel (Figure 2.5). Analyzing every imaginable (or combination of) feature(s) means costly computation of meaningless and sometimes redundant information. Therefore we consider only those features meaningful for our segmentation purposes and that don't overlap within each other (Figure 2.6). The selected components are:

- Luminance ***L*** -as the sum of the red, green and blue channels- characterize the brightness (as energy) of a texel (Figure 2.6(b)).

- ***R-G*** and ***R-B*** represent the difference of the red channel with the green and the blue one, respectively. These differences not only reduce the effect of specular skin highlights but also relate the green and blue components to the red one. The red component is dominant in hair regions due to the presence of blood flows in the dermis, independent of skin color (Figure 2.6(c) and 2.6(d)).

- The absolute value of the local texture gradient $\boldsymbol{g}$ helps to discriminate between rather smooth ("low frequency") skin and less homogeneous ("high frequency") hair regions (Figure 2.6(e)).
- "strength of orientation" $\boldsymbol{o}$ in the texel. Hair regions tend to have a predominant growth direction, at least on a texel scale (Figure 2.6(f)).

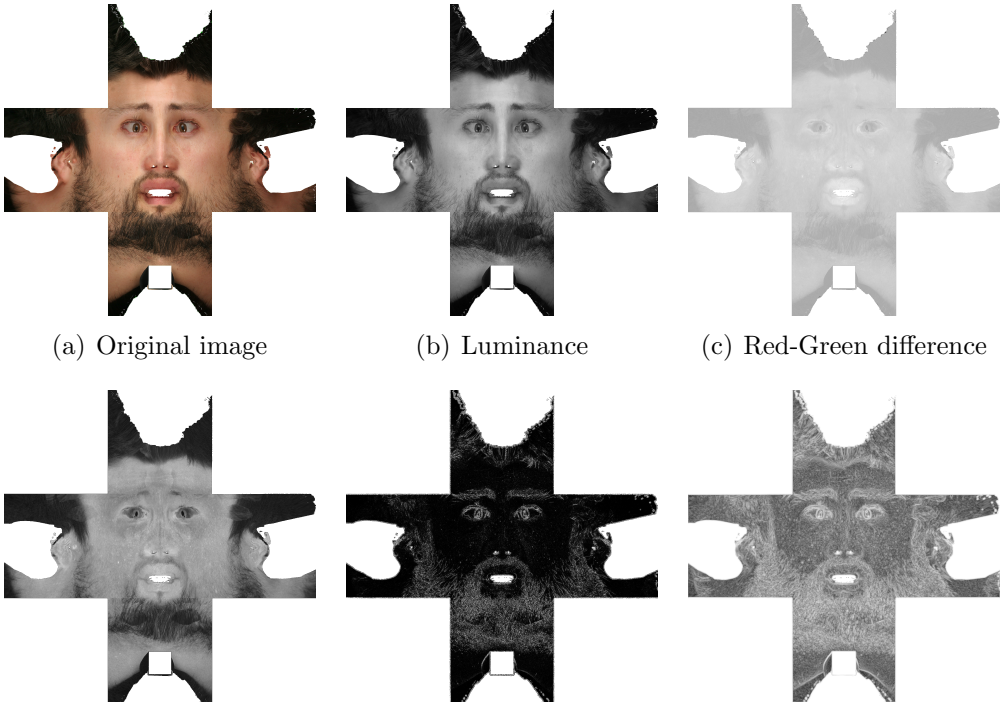

(a) Original image (b) Luminance (c) Red-Green difference

(d) Red-Blue difference (e) Module of gradient (f) Orientation's strength

Figure 2.6: Separated view of the components of the feature vector.

2.2.2 Discriminating Skin and Hair –An Iterative Approach

We now use the above introduced feature vector to compute $p_{\text{hair}}^{(i,j)}$. To do that we assume that the typical characteristics of both hair and skin can be sufficiently well characterized by small "exemplary" learning regions in the texture of S and proceed iteratively as follows.

1. Two square blocks –one for skin and another for hair– are selected randomly in the texture image.

2. A group of histograms, one per feature, is generated for each block using the information stored in the texel-calculated feature vector (Figure 2.7).

3. A Bayesian estimator calculate $p_{\text{hair}}^{(i,j)}$ using the generated histograms.

4. A measure that estimates the quality of the block's selection is computed.

After the above described procedure is repeated an user-defined number of times, the best result with respect to the computed measure is kept. This approach is explained in detail in the following section

Calculating $\text{p}_{\text{hair}}^{(\text{i,j})}$

Let $\widetilde{H}$ and $\widetilde{S}$ denote the randomly selected learning regions for skin and hair and $\left|\widetilde{H}\right|$ and $\left|\widetilde{S}\right|$ their corresponding cardinalities.

We start by computing an initial estimate $\mu_{\text{hair}}^{(i,j)}$ ($\mu_{\text{skin}}^{(i,j)}$) for the probability of a texel $t_{(i,j)}$ for belonging to hair (skin) region, according to our feature set $X = \{x_k\}$, with k indexed over the features $\{L, R-G, R-B, g, o\}$. These estimators will be used in a subsequent step to calculate the final probability values (equation 2.6).

The computation of these estimators is not straightforward. The feature vectors $X^{(i,j)}$ are multidimensional and dealing with them in a direct manner is unpractical due to the order of magnitude times feature space samples (provided by the two skin and hair learning regions) required to obtain meaningful statistical results. Therefore all statistic are first computed independently for each of the components $x_k^{(i,j)}$ taking a Bayesian estimation approach and then combined to finally obtain the posterior probability $p_{\text{hair}}^{(i,j)}$.

Suppressing the (i,j)-dependence and using Bayes formula the following holds:

$$\mu_{\text{hair}}^{k} = P(\text{hair} \mid x_k = h_k^n) = \frac{P(\text{hair} \cap x_k = h_k^n)}{P(x_k = h_k^n)} \tag{2.1}$$

where h_k^n is denoting the n-th bin in the corresponding x_k-histogram h_k.

Substituting with $\left|\widetilde{H}\right|$ and $\left|\widetilde{S}\right|$ yields

$$\mu_{\text{hair}}^k = \frac{\frac{\left|\widetilde{H}_{(x_k=h_k^n)}\right|}{\left|\widetilde{H}\cup\widetilde{S}\right|}}{\frac{\left|\widetilde{H}_{(x_k=h_k^n)}\cup\widetilde{S}_{(x_k=h_k^n)}\right|}{\left|\widetilde{H}\cup\widetilde{S}\right|}} \tag{2.2}$$

and after eliminating denominators we arrive at

$$\mu_{\text{hair}}^k = \frac{\left|\widetilde{H}_{(x_k=h_k^n)}\right|}{\left|\widetilde{H}_{(x_k=h_k^n)}\cup\widetilde{S}_{(x_k=h_k^n)}\right|}. \tag{2.3}$$

The probability estimates μ_{hair}^k are then combined by the following weighted average heuristic taking into account the spread of the histograms h_k:

$$\frac{1}{\sigma_{\text{hair}}^2} = \sum_k \frac{1}{\sigma_k^2} \tag{2.4}$$

$$\mu_{\text{hair}} = \frac{1}{\sigma_{\text{hair}}^2}\sum_k \frac{\mu_{\text{hair}}^k}{\sigma_k^2}. \tag{2.5}$$

Here, σ_k is denoting the normalized standard deviations[1] of the histograms h_k.

Although this simplistic approach is optimal for combining Gaussian probability densities only, it works surprisingly well in our case. An expression for μ_{skin}^k can be derived similarly.

The results of applying (2.5) $\mu_{\text{hair}}^{(i,j)}$ and $\mu_{\text{skin}}^{(i,j)}$ contain complementary information about the distribution of facial hair. Ideally, the two values should sum up to one, for each texel $t_{(i,j)}$. Considering this property the probability estimates can be improved further by combining $\mu_{\text{hair}}^{(i,j)}$ and $\mu_{\text{skin}}^{(i,j)}$ according to:

$$p_{\text{hair}}^{(i,j)} = \sqrt{\mu_{\text{hair}}^{(i,j)} \cdot (1 - \mu_{\text{skin}}^{(i,j)})} \tag{2.6}$$

[1] The standard deviations are normalized by the range of feature values present in the texture of the source S.

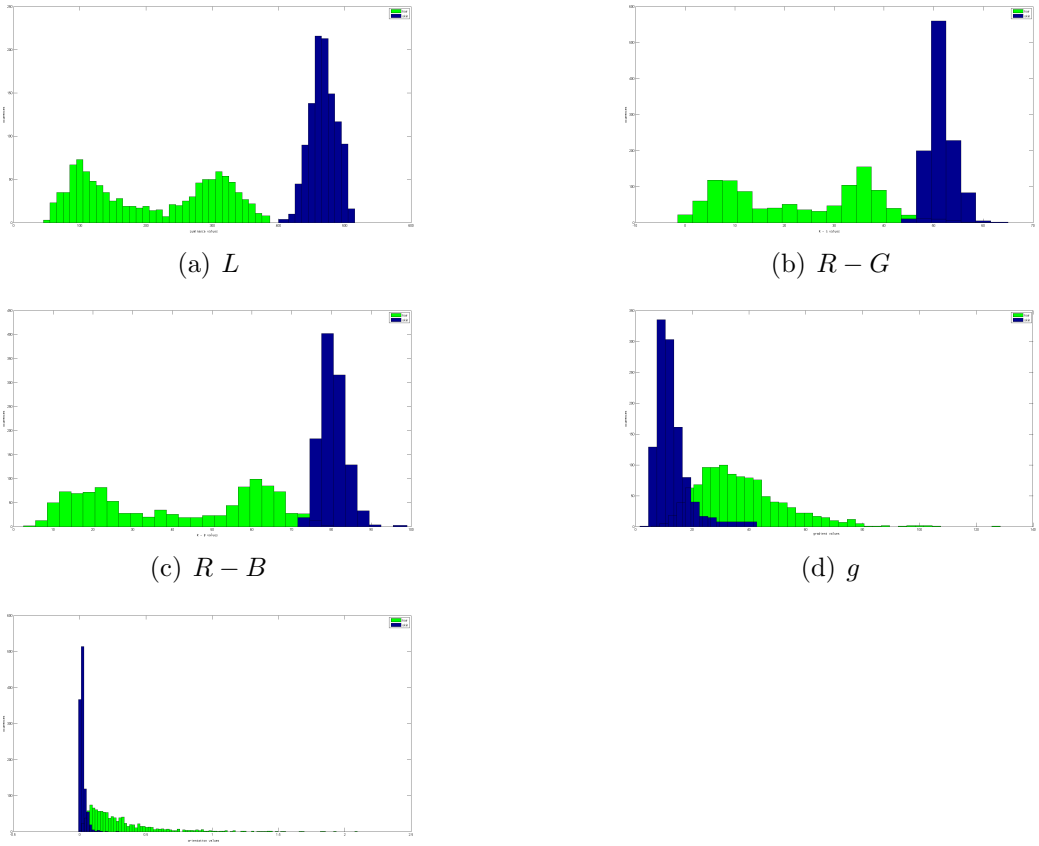

(a) L (b) $R - G$

(c) $R - B$ (d) g

(e) o

Figure 2.7: Typical histograms h_k for each of the feature set components x_k derived from the selected hair(green) and skin(blue) regions. Please note their difference in distribution.

$$p_{\text{skin}}^{(i,j)} = \sqrt{\mu_{\text{skin}}^{(i,j)} \cdot (1 - \mu_{\text{hair}}^{(i,j)})}. \tag{2.7}$$

The probabilities $p_{\text{hair}}^{(i,j)}$ are used to characterize the distribution of facial hair.

A Quality Measure for Classification

The sequence of steps described above is repeated an user defined number n of times and in each iteration $k \in \{1, .., n\}$ the probabilities $p_{\text{hair}}^{(i,j)}$ are computed according to the selection of hair and skin learning regions. The only constraint to the random learning regions selection process is that the

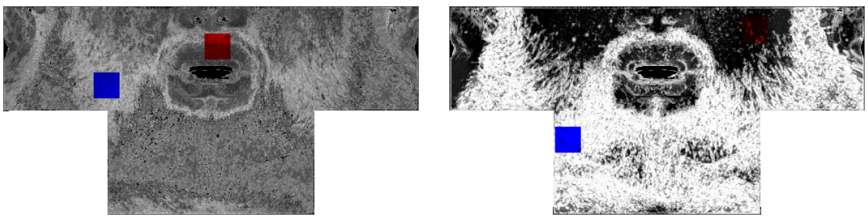

(a) Bad selection (b) Good selection

Figure 2.8: Resultant probability maps. Randomly selected learn regions are marked in red and blue.

chosen regions lie completely inside the texture image. From the two regions, the one with the lowest gradient g, averaged over all its texels, is declared as hypothetical "skin". To identify the optimal selection a simple but efficient heuristic is used, calculating for each selected pair of regions the distance between texels marked as "hair" and their "skin" counterparts.

Assuming that a selection is suitable if a clear classification (as either hair or skin) is possible, the quality measure m^k is computed as follows:

$$m^k = \sum_{i,j} \max(p_{\text{skin}}^{(i,j)}, p_{\text{hair}}^{(i,j)}). \tag{2.8}$$

The value m_{best} is given for the iteration (i.e. the pair of regions) that maximizes the separation of assumed skin and hair texels (Figure 2.8):

$$m_{\text{best}} = \max(m^1, .., m^n). \tag{2.9}$$

For all our tests $n = 2048$ was used. This number was not selected randomly but is an optimal trade-off between the size of the learning regions, the size of the texture images and the run-time of the algorithm.

2.2.3 Estimating the Growth Direction of Hair

After the location of the facial hair has been estimated, the next step is to calculate the direction in which these hairs grow. For that we compute a 2-D vector field (Ω) over the texture image that represents the hair's predominant

growth direction (Figure 2.9).

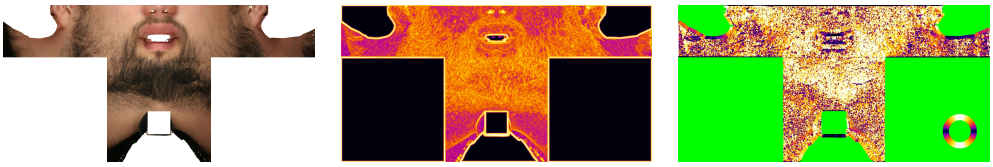

Figure 2.9: Orientation information (right) extracted from a beard image (left). The confidence of the orientation information (middle) is measured according to the response of the orientation filter.

In order to achieve this we use the "steerable filters" method, as proposed by Freeman and Adelson [FA91, Fre92]. Following this approach a filter is defined by a kernel K designed to detect an x-aligned orientation. To test an arbitrary rotation in pixel (i, j) the convolution of K_θ –K rotated by θ– is computed. The "oriented energy" of the convolution, used to characterize the strength of orientation, is given by:

$$E_2(\theta, i, j) = [G_2^\theta(i, j)]^2 + [H_2^\theta(i, j)]^2 \tag{2.10}$$

where G_2 is the second derivative of a bi-dimensional Gaussian function and H_2 is its corresponding Hilbert transform.

Dividing the interval $[-\pi/2, \pi/2)$ in equally spaced angles and testing the filter for each of these angles yields a "response curve" for each texel $t_{(i,j)}$. The maximum of the response curve indicates the predominant orientation $\Omega^{(i,j)}$ and its confidence $\omega^{(i,j)}$ is computed as the inverse of the curve's variance [PBnS04].

In the following p_{hair} and Ω will be summarized by a vector Γ that contains all information extracted from S:

$$\Gamma = \begin{bmatrix} p_{\text{hair}} \\ \Omega \end{bmatrix}. \tag{2.11}$$

2.3 Generation of a Statistical Prior

After extracting the hair region and estimating its orientation we have in Γ all the information needed to synthesize facial hair. Still, sometimes the collected data is not sufficient to perform the synthesis of facial hair. Texture images can be noisy or have overshadowed areas. Moreover, in some cases the texture generation algorithm [PKA+09] cannot solve discontinuities between image patches. These issues have a direct negative impact in the reliability of the estimated probability map and orientation vector field. In those cases Γ may be improved by taking into account statistical information about p_{hair} and Ω obtained from many individuals. For that, a statistical prior is computed from a database of registered texture images $I_k, k \in \{1, .., n\}$ from reliable models (Figure 2.10).

We start by computing the corresponding Γ_k distributions from the database texture images and combining them to a "prior" $\bar{\Gamma}$ by weighting averaging:

$$\bar{\Gamma} = \begin{bmatrix} \bar{p}_{\text{hair}} \\ \bar{\Omega} \end{bmatrix} \tag{2.12}$$

with

$$\bar{p}_{\text{hair}} = \frac{1}{\sum_k m^k_{\text{best}}} \sum_k m^k_{\text{best}} p^k_{\text{hair}} \tag{2.13}$$

and

$$\bar{\Omega}^{(i,j)} = \frac{1}{\sum_k \omega^{(i,j)}_k} \sum_k \omega^{(i,j)}_k \Omega^{(i,j)}_k. \tag{2.14}$$

Please note that the weights for $\bar{p}_{\text{hair}}$ –which are constant for all texels of I_k– are given by the optimal quality measure used for hair/skin classification. Thus, results p^k_{hair} with a clear separation of skin and hair regions tend to influence the final result of $\bar{p}_{\text{hair}}$.

In contrast to $\bar{p}_{\text{hair}}$ the weights for $\bar{\Omega}^{(i,j)}$ are computed on a local basis. Here we use $\omega^{(i,j)}$ that characterize the confidence of the image orientation in a local way, implying that strongly oriented pixels are most relevant to the prior.

The generated $\bar{\Gamma}$ is used to improve the already estimated distributions

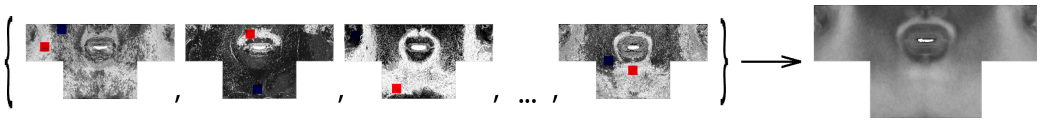

Figure 2.10: A "prior" is used to improve the estimated facial hair distribution p_{hair} of a target T in case of missing or incomplete information as well as to avoid "false positive" hair texels. This prior (rightmost image) is based on a database of over 70 individuals and statistically combines relevant features present in the dataset. In each texture the red and blue blue blocks indicate the best pair of "learning regions" found by our iterative optimization process.

Γ_k in a local fashion.

The goal of improving Γ_k is to accentuate the separation between the hair and skin texels while keeping relevant detail of the originals and completing regions that are not well classified as either skin or hair. Intuitively, this means that regions of high uncertainty are enhanced with prior data whereas texels that have been clearly identified as skin or hair are nearly preserved.

This objective is achieved by applying the prior as follows:

$$\begin{aligned} p_0 &= \min(p_{\text{hair}} \cdot \bar{p}_{\text{hair}}, \bar{p}_{\text{hair}}^2) \\ p_1 &= \max(p_{\text{hair}}, \sqrt{p_{\text{hair}} \cdot \bar{p}_{\text{hair}}}) \\ p'_{\text{hair}} &= \begin{cases} p_0 & 1 - p_0 > p_1 \\ p_1 & \text{otherwise} \end{cases} \end{aligned} \tag{2.15}$$

Using two different expressions p_0 and p_1 allows for accentuating the difference between skin and hair which is especially important for avoiding "false positive" hair regions (Figure 2.11).

To improve the orientation map we follow a different approach, because the goal is to improve the angle measurement. Therefore, from the estimated angle ($\Omega_k(i,j)$) and the combined one ($\bar{\Omega}(i,j)$) we select the one with the largest confidence value.

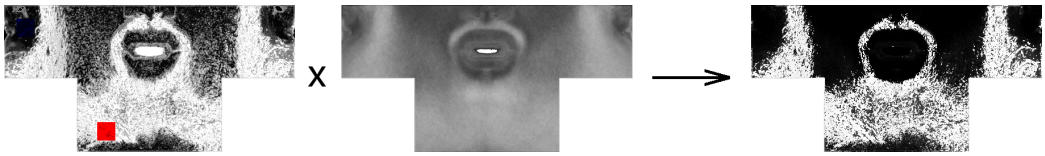

Figure 2.11: Combining the original probability distribution p_{hair} (leftmost image) with the prior (middle image). This operation allows for a much clearer separation of skin and hair ensuring that all features of the original probability map are also present in the resultant chart (rightmost image).

2.4 Facial Hair Synthesis

After improving Γ we know accurately where and in which direction the facial hair grows. To be able to synthesize the hair geometry, we first have to transfer all the information extracted from the two-dimensional image space to the three-dimensional model space. Since the texture images are registered, a direct correspondence between image- and model-coordinates can be established. Therefore the transfer of information to the model's surface is very simple.

2.4.1 Distributing Hair Roots

The first step of the synthesis stage involves the computation of the filament root locations. Following a *direct* approach we take advantage of the size of the texture image T and count the hair roots on the extracted hair region, whereas an *indirect* approach estimates the location of the roots using the probability map p_{hair}.

To count the hair roots we start by delimiting the facial hair region on the texture image using graph cut [BK04] based on the probability chart. We then apply a blob detector, adapted to the projected size of the roots in the images, to detect the hair roots in the delimited region. An advantage of this alternative is that we are actually generating hair exactly where T should have it. However this approach fails in many cases. Although the resolution of the texture image allow us to detect structures with the size of the roots, the technique works only in fresh shaved models and even in those cases the

inherent distortion of the textures due to the form of the head causes the approach to fail.

To avoid these issue we estimate the location of the roots based on the probability map. Let n be a user defined parameter specifying the number of filaments to be synthesized, a 2D sampler distributes n samples using p_{hair} as probability density function (pdf). These samples are then projected from image space to model space. For the i-th filament the resulting 3-D position of its corresponding root is denoted $\vec{P}_{\text{i}}$.

2.4.2 Generation of Filaments

The hair filaments are generated using a "particle shooting" approach: the shape of the filament is described by the trajectory of a "projectile" that is "shot" from the hair root $\vec{P}_{\text{i}}$ with an initial spatial orientation $\vec{O}_{\text{i}}$. Based on the one-to-one correspondence between image and model coordinates, the initial orientations are calculated by projecting Ω onto T's head model and computing for each 2-D image orientation vector a 3-D vector parallel to the head surface, originated on the corresponding head model vertex. Having a spatial orientation for each vertex, we calculate for each root position $\vec{P}_{\text{i}}$ its underlying triangle in the head model triangle mesh and obtain $\vec{O}_{\text{i}}$ by interpolation of the orientation in the triangle vertices. To further improve the results we add a gentle pseudo gravity force $\vec{f}_g$.

In order to obtain plausible results we also take filament-filament as well as filament-head model collisions into consideration during the filament growth phase. Collisions are detected by a grid based approach [THM+03]. The filaments are generated starting at the roots by an iterative synthesis process, extended in each iteration according to the particle trajectories. Collisions are avoided by separating filaments that are in contact. Thanks to the way the filaments are generated (all grow at the same time) we can resolve collisions simultaneously for all filaments within a certain predefined neighborhood.

Generation of Eyebrows

Eyebrow filaments are generated differently because they tend to be more aligned. For that reason no particle shooting is applied. Instead the 2D orientation field Ω is used directly as filaments growth direction. Starting at the 2-D root location in texture space the filaments are tracked through Ω. The resulting trajectories are then converted to 3-D model space and are terminated as they reach a predefined maximum length.

2.4.3 Rendering

The realistic visualization of the resultant geometry is the last step of the modeling process. In order to achieve physically-plausible results the hair shading framework proposed by Zinke and Weber [ZW07] was used. It is important to note that believable results are obtained only if the rendered hair exhibits similar detail as the textures mapped onto the 3D head models. This is obtained by adapting the filter width used for image reconstruction (as final part of the rendering pipeline) to the size of projected texels in image space.

2.5 Results

Figure 2.12 illustrates through a simple example the different stages of our pipeline, whereas Figures 2.13 and 2.14 show two applications of our approach.

Beard Transfer In Figure 2.13 facial hair is characterized from different sources (topmost row) and transferred to several hairless targets (leftmost column). The combination of our approach with techniques like *Morphable Head Model* [BV99] yields very pleasing results, since the addition of facial hair increases considerably the level of realism of the synthesized 3-D faces. By combining both techniques the question of *"how Beethoven would look like with my beard and my eyebrows ?"* can be answered.

Figure 2.12: Stages of the facial hair generation process. Starting with the 3D head model and texture images as input data (first and second images from left), the facial hair region is estimated using a probability map (middle image), the hair filaments are generated with their corresponding distributions and orientations (fourth image from left) and finally a photo-realistic image is rendered (last image).

Prior-based Facial hair generation As shown in Figure 2.14 our approach generates plausible beards on (nearly) completely shaved individuals (leftmost column). Taking advantage of the statistical prior in conjunction with the texture images we are able to synthesize believable results (rightmost column) even in very challenging cases. The resulting hair distribution is very consistent with original regions which are hardly visible in the texture images. For comparison purposes also the pure prior was transfered to the models (middle column).

Not only the generation of realistic virtual avatars but also other fields benefit from our approach: based on a photo of a shaved person and the *Morphable Head Model* our technique can be used to infer how this person would look like if he had a beard or mustache. This application can be very useful in fields like criminal sciences.

The most obvious limitation of our approach is that it is based on the assumption that a mapping between the 2-D texture space and the 3-D model space is known. That restricts our input data to registered texture images. Other limitation is that the textures in the database must be similar in order for the prior to be constructed in a meaningful way.

Feature detection is the most time-consuming step of the whole process. With an Intel Core 2 Duo CPU (E8500 @ 3.16 GHz, using a single core), it takes around 45 seconds to process one model. This feature detection is required also for each of the models that are used to build the statistical prior. However, since the prior is computed only once and remains unchanged for

all subsequent analysis, its cost (50 minutes of pre-computation our case) is usually not a limiting factor.

The other time consuming step is the geometry synthesis, whose runtime depends strongly on the number of filament to be generated. All of our examples have 11000 filaments with 10 mm maximal length each. With these parameters the hair geometry is generated in 25 seconds.

2.6 Conclusions

We have presented a technique that successfully extracts the geometric information of facial hair out of registered 2D textures and uses it for different synthesis tasks on (morphable) 3D-head models (Figures 2.13 and 2.14).

As for the existing approach a very simple heuristic was used to determine the length of a filament. An interesting topic of future work would be to infer this length directly using more sophisticated texture space analysis as well as database statistics.

We did not attempt to extract "hair color" information from the images. Notice that "hair color" is a concept that must be defined carefully on the fiber level, e.g. as the parameters of a BCSDF scattering model [ZW07, ZRL+09].

Zinke et al. [ZRL+09] present a practical approach for the acquisition of hair color (the parameters of the BCSDF of an average fiber) of scalp hair out of images. This approach requires that a hair strand is wrapped around a cylinder to have a well defined hair geometry with "good" properties for solving the inverse rendering problem. Whereas this approach is not directly applicable to facial hair, the more regular geometric properties of facial hair with respect to scalp hair makes it plausible that this approach can be adapted to the problem of BCSDF estimation of facial hair fibers.

The ultimate goal of our future work is aimed to extend our technique to the development of an approach that allows the modeling of complete hairstyles using qualitative information retrieved from images.

Figure 2.13: Beard transfer. Two different sources (topmost row) are used to synthesize beards on four different targets (leftmost column). Beethovens's foto courtesy of Beethoven-Haus Bonn.

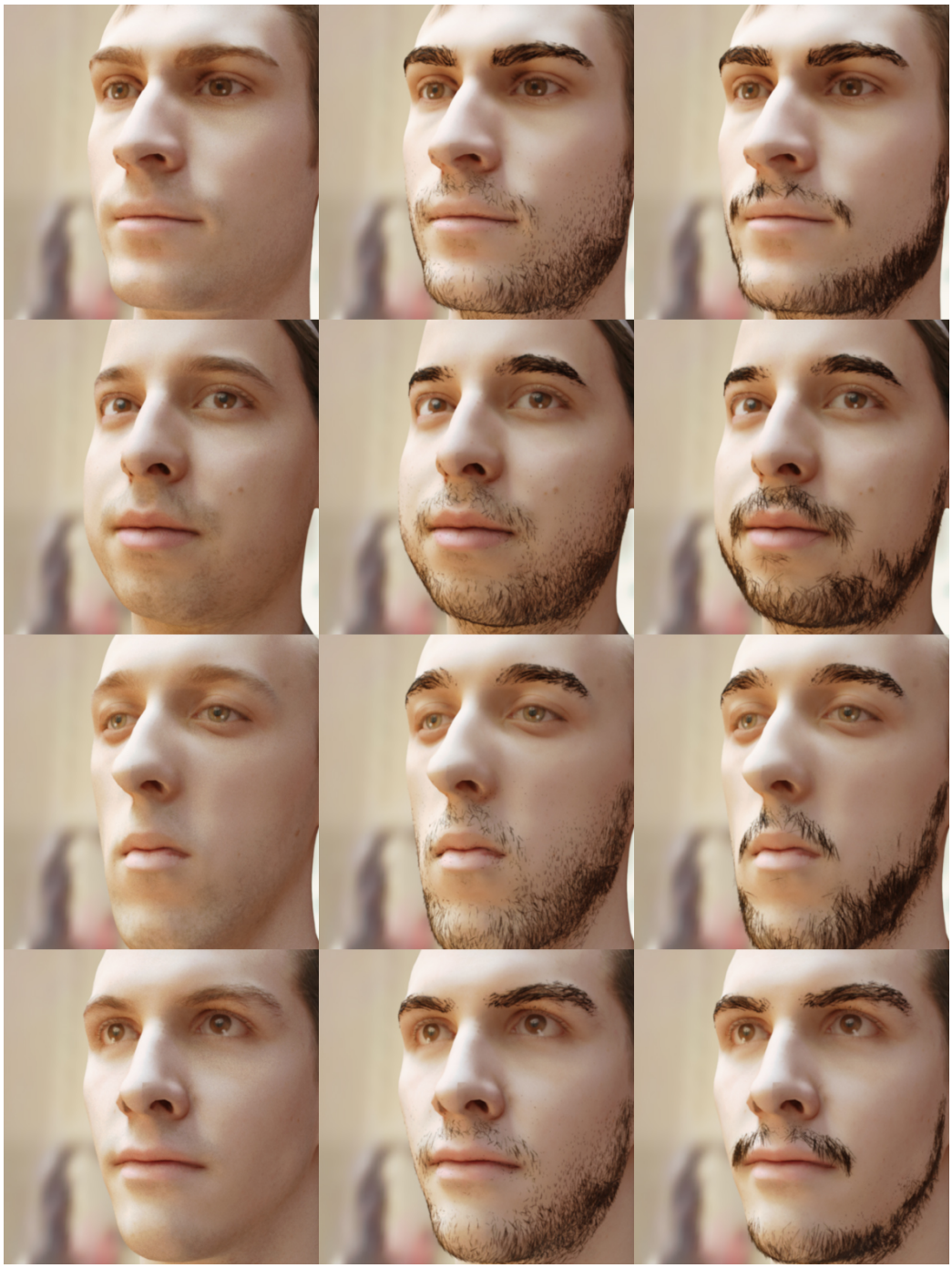

Figure 2.14: Applying our method to shaved individuals (first column). Results obtained by using exclusively information from our statistical prior (middle row) and the final results also taking into account the specific characteristics of individuals according to the full pipeline (rightmost row).

3

Thermal-Based Hairstyle Modeling

In this chapter we describe an approach to model fiber-based hairstyles using thermal images (thermograms). Our reconstruction technique takes as input a sequence of images obtained with an hand-held thermal camera and synthesizes a fiber-based hair geometry that resembles the captured hairstyle.

3.1 Introduction

Because of its influence on the human appearance, plausible hair plays a crucial role in the creation of digital avatars. Therefore the development of robust and efficient techniques for the generation of realistic hairstyles is still a relevant topic in the computer graphic community, despite being treated several times in the past [AUK92, WBK+07, HCL+07, BHC+08].

Modeling human hairstyles, however, is a very challenging task. The human brain is extremely well trained in recognizing hair under different conditions, therefore even slightest errors may lead to visually unconvincing

results. On the other hand the geometrical complexity of hair is a serious issue. A typical human hairstyle consists of approximately 100000–150000 long and thin filaments, whose shape is a result of complex fiber-fiber interactions and the effect of cosmetic products.

Therefore, the majority of hairstyle modeling techniques published to date rely on manual work, requiring special skills from the user to obtain satisfactory results [KN00, KN02, WLL+03, YSK09]. In order to reduce the degree of manual work, some approaches generate hairstyles with the help of physical models describing the behavior of hair strands [HMT00, BAQ+05, CK05, SKW06]. Instead of synthesizing new hairstyles, image-based techniques attempt to reproduce existing hairstyles using information extracted from images [PBnS04, WOQS05, PCK+08, JMM09].

Although generally simpler and less interaction dependent than other approaches, image-based techniques are not exempted from limitations: While some require a very complex acquisition setup with controlled lighting conditions and multiple cameras [PCK+08], other require substantial manual pre-processing, e.g. for hair-skin segmentation, to obtain acceptable results [WOQS05]. Moreover, they are likely to give unreliable results in cases where global optical effects –e.g. self-shadowing or strong multiple scattering– cannot be correlated with local shape. The fact that classical image-based approaches can only image the surface of a hair volume but give no insight about the inner volumetric structure represents another limitation.

Following previous image-based work and attempting to overcome the above mentioned limitations we present in this chapter a novel, fast and more robust approach for reconstructing a given hairstyle from video streams taken with an infrared camera. The key idea is to use far infrared imaging to overcome most of the issues related to the visual range. Compared to classical imaging, far infrared imaging has several advantages (Figure 3.1):

- With the head acting as “light source” illumination-related issues, such as shadowing, are avoided.
- As heat is irradiated from the head almost isotropically, the captured temperatures in the hairstyle surface are viewpoint independent.

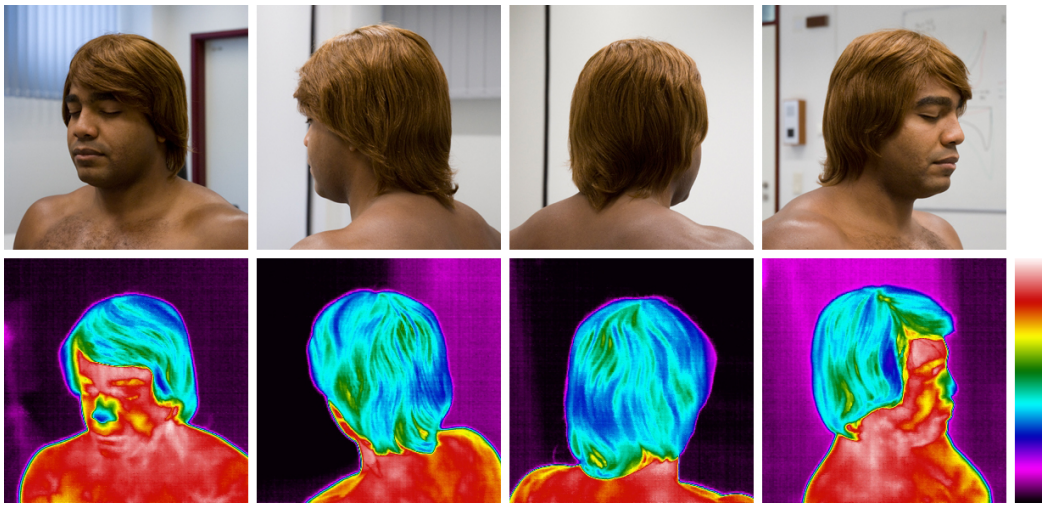

Figure 3.1: Conventional and thermal images of a model wearing a wig. The thermal images show hairstyle features not clearly visible on the conventional images due to poor illumination or shadowing.

- The hair-skin segmentation becomes a trivial task, based on the temperature distribution of the captured scene.

- A dedicated photo-consistency-based approach can be used for capturing full hairstyles under arbitrary lighting conditions using a single hand-held thermal video camera.

To improve the accuracy and computational efficiency of the reconstruction process we extend existing state-of-the-art techniques along several lines. Besides an extremely simple data acquisition setup, the main contributions of our hairstyle reconstruction pipeline are:

- The reconstruction of the hairstyle boundary based on photo-consistency is accelerated by at least one order of magnitude thanks to the local relationship between temperature and distance to the skin. This enables us to increase the resolution of the reconstructed boundary.

- Local image orientation is computed using a multi-scale orientation analysis approach. The accuracy of the extracted information leads to

a more robust estimation of local hair orientation, a key component for synthesis of the hair geometry.

- Opposed to previous methods in which hair is generated starting at the scalp, filaments in our approach are synthesized starting at the most reliable regions of the hairstyle boundary. Moreover, we propose a novel two step approach for synthesizing individual hair strands where more reliable data is considered first and smoothness and curvature constraints help to recover continuous strands. This latter step is extremely useful when modeling curly hair.

In the following sections we provide a summary of state-of-the-art techniques for hair modeling as well as a description of the theory behind our approach and a detailed description of every step in our pipeline.

3.2 Related Work

According to Ward et al. [WBK+07] hair modeling techniques can be classified with respect to required input as either geometry-based, physically-based or image-based.

3.2.1 Geometry-Based Hair Modeling

Approaches under this category use geometric features (e.g. curves) to represent hairstyles and are highly dependent of user interaction. An average hairstyle has more than 100000 hair filaments and modeling each one of the hair fibers separately is an extremely tedious and time consuming task. Fortunately, adjacent hair strands tend to form wisps and behave in a similar way [WS92]. Following this idea, only a set of hair strands ("guide strands") are modeled by hand, while the rest of the filaments is generated by interpolation techniques. The information defining a hairstyle is usually coded in a level-of-detail (LOD) structure to further simplify the modeling process.

A common approach to reduce the number of objects needed to model a section of hair is to represent groups of strands by two-dimensional *parametric*

surfaces [KN00, LH03, NT04]. These "hair strips" are characterized by a location on the scalp, orientation and a group of weighted knots defining the hair shape. Hairstyles can be modeled with relative ease by specifying control curves and connecting its control points to create hair strips. The flat representation of the strip, however, limits the types of hairstyles that can be modeled.

To alleviate this issue, Liang and Huang [LH03] warped the 2D surfaces to U-shaped meshes, giving thus more volume to the hair. The U-shapes are obtained by connecting the vertices of the hair strip with its projections on the scalp. Kim and Neumann [KN00] proposed a method in which hair strips generated from parametric surfaces are offset along its normal direction, forming a "Thin Shell Volume" (TSV). Hair filaments are then generated inside the volume. The approach followed by Noble and Tang [NT04] fills a volume of parametric surfaces defining the shape of the hairstyle with clumps of hair geometry created from profile curves extruded along the length of key hairs.

A comprehensive and highly interactive tool for hairstyle modeling using polygonal surfaces was presented by Yuksel et al. [YSK09]. With the help of "Hair Meshes" users can directly control of the overall shape of the hairstyle, being thus able to accurately model any desired shape.

Some approaches describe the volume surrounding a guide strand by *wisps* or *generalized cylinders* [CSDI99, XY01, PBL04, CK05]. This intuitive representation of a group of hair strands reduces the number of parameters needed to model a hairstyle, as strands are grouped around a space curve acting as centerline of the generalized cylinder, or cluster. The shape and position of the centerline as well as the distribution and shape of the strands inside the cylinder are controlled interactively.

Chen et al. [CSDI99] present a system to generate hairstyles based on a trigonal wisp model and the shape of the hair filaments inside the wisp is determined by a 2D distribution map in every cross-section of the wisp. The approach followed Xu and Yang [XY01] develops an interactive hair-design system based on a cluster hair model in which filaments are generated according to a distribution map swept along the axis curve defining the shape of the generalized cylinder. The axis curves are generated interactively

and the distribution maps are generated randomly at the base cross-section of the cylinder. Patrick et al. [PBL04] classify african hairstyles in curly, straightened or braid and twists. While curly hair is modeled using implicit methods, the latter two are modeled using a cluster method by specifying position and shape of control hairs. Hairstyles generated by the technique presented by Choe and Ko [CK05] are based on a statistical wisp model and a pseudo-physical deformation solver that accounts for the effects of gravity and collisions in a simplified way.

Considering the fact that in a human hairstyle adjacent hair strands tend to form clusters at different scales, Kim and Neuman [KN02] presented a *Multi-resolution Hair Modeling* (MHM) system. Following this approach a hairstyle is modeled using a hierarchy of generalized cylinders where coarser levels describe the overall appearance of the hairstyle and finer levels represent individual hair strands. On the other hand, Ward et al. [WLL+03] model hair using level-of-detail representations. Hair structures can be classified as either individual strands, hair clusters or hair strips, and a hierarchy of subdivision curves or surface representing the structures is used to model the hairstyle.

Due to its high degree of user interaction, all the above mentioned approaches can only be meaningfully used by highly skilled 3D artists, and even in those cases the modeling process can be very tedious and time consuming.

3.2.2 Physically-Based Hair Modeling

Approaches under this category attempt to model a hairstyle according to the hair's physical properties, or try to recreate the features of a hairstyle by parameterizing hair volumes. Physically-based modeling techniques require less information regarding the hairstyle to be modeled and are less dependent on user interaction than its geometric-based counterparts.

In the work of Anjyo et al. [AUK92] hair filaments are modeled as *cantilever beams* –straight beams fixed at one end– as hairs are anchored at the scalp and have the other end free. The rest position of the filaments is calculated by simulating the statics of a cantilever beam, where gravity is the main

source of hair bending, and accounting for collision detection between hairs and the head. Cutting operations and final adjustments based on additional forces are used to give a realistic appearance to the filaments.

Based on the visual similarities between human hair and *fluid flows*, Hadap and Magnenat-Thalmann [HMT00] present a styling tool in which hair strands are modeled as streamlines of a stable fluid flow. By manually placing flow elements –sink, vortices and sources– large scale properties as well as fine details of the hairstyle can be controlled.

Bertails et al. [BAQ+05] propose a technique closely related to the *mechanics* of hair fibers. Here the static behavior of hair fibers is modeled based on the Kirchhoff model for static Cosserat rods, which accounts for the main features of hair, such as natural curliness or ellipticity. The equilibrium shape of the hairstyle is computed by energy minimization. Wither et al. [WBC07] uses a similar technique to model hairstyles based on user-defined sketches.

The mechanical model presented by Sobottka et al. [SKW06] is based on the Cosserat rods as well. This approach searches for the "optimal" force-torque combination that deforms the hair filament in such a way that it conforms to a given hairstyle boundary ("hull" shape) and additional hair density information, using physically accurate parameters and accounting for hair-hair collision response.

Hairstyles and *vector fields* have in common that they are volumetric data and have a clear orientation at specific points. Considering that, Yu [Yu01] uses static vector fields to model hairstyles. A global field is generated by superimposing procedurally defined vector field primitives that have local influence. An initial hair model is extracted from the superimposed vector field by tracing their field lines and random curliness can be added to the model by a parametric hair offset function.

Fu et al. [FWTQ07] propose a method in which a hairstyle is modeled by 3D style curves inside the hairstyle bounding volume. The style curves are created interactively via drawing free-form strokes and a discrete vector field is generated within the bounding volume, in which boundary constraints are derived from the sketched curves. Hair filaments are then synthesized following the generated vector field, starting from a given scalp region.

Choe et al. [CK05] also uses a vector field to compute the final position of the hairs. Their hair deformation solver traits hair as a continuum and computes the global position of the strands according to an unified force field accounting for gravity and styling operations, such as ponytails or hairpins. An additional density field is used to handle collision detection.

Physically-based modeling techniques are not so dependent on user interaction and therefore easier to use by the final user. However, this reduction of user interaction can be seen as a limitation, as the control of the user over the resulting hairstyle is limited as well. Another limitation of such approaches is that, being physically-based, they generally rely on a set of parameters whose fine tuning can be very complex.

3.2.3 Image-Based Hair Modeling

Conventional image-based techniques recreate hair geometry based on pictures taken from the hairstyle to be modeled. Opposed to geometric- or physically-based approaches, image-based techniques require minimal user interaction, since all required information is extracted from the images. This can be seen as an advantage, since no special skills are needed to model a hairstyle, or as a drawback due to the lack of freedom the user has during the modeling process.

The first attempt to model a hairstyle from images was presented by Kong and Nakajima [KN98]. In their approach the 3D hairstyle volume is computed from photos of the subject's hair taken at various viewpoints. Filaments inside the volume are generated following a heuristic that does not necessarily reproduce the shape of the captured hair but gives pleasant results when modeling simple hairstyles.

In the approach proposed by Grabli et al. [GSML02] the hair is analyzed from a fixed viewpoint under varying illumination conditions to estimate the orientation of the hairstyle surface. Fixing the viewpoint allows to work with perfectly registered images, but at the same time drastically limits the quality of the reconstruction as only part of the hairstyle is visible.

Following a similar idea, Paris et al. [PBnS04] extended the experiment

incorporating four fixed viewpoints and many known lighting directions to create a full hair model. First the hair shape is approximated using a visual hull computed from manually segmented images into hair and non-hair regions. Subsequently, an orientation vector field of hair strands is calculated by testing different filters on a given 2D location and selecting the one giving the most reliable response for that location. To obtain 3D directions a dedicated shape from shading approach is taken. Finally, hair growth starts at the scalp using explicit numerical integration with a force field computed from interpolated orientations. This growth stops when filaments reach the boundary of the visual hull.

Wei et al. [WOQS05] presented the first attempt to reconstruct a hairstyle using a handheld camera under unconstrained illumination conditions, demonstrating that it was possible to accomplish the task without need of a complicated setup, only by exploiting the geometry constraints of multi-view reconstruction. Like Paris et al. [PBnS04], the reconstruction is based on a visual hull of the hairstyle computed using manually segmented silhouettes. Since they are based on visual hull, both the methods of Paris et al. [PBnS04] and Wei et al. [WOQS05] suffer from general limitations. They rely on visual hull, therefore concavities cannot be modeled correctly and massive user interaction is required to segment hair and non hair regions. This is especially true for Wei et al. where no corrective (such as shape from shading) is available.

A more sophisticated approach to really reconstruct a hairstyle down to the hair filament level was proposed by Paris et al. [PCK+08]. The acquisition setup consists of a dome-like structure containing 3 DLP (Digital Light Processing) projectors, 16 Basler cameras and 150 LED light sources. The projectors and cameras are calibrated and the position of the light sources is known. Based on triangulation from structured lighting both shape and shading are acquired. Although the results are impressive, the hardware requirements, the time for acquisition as well as the computational costs are extremely high.

Another technique to reconstruct hair with filament-level accuracy, however in a considerably smaller scale, was presented by Jakob et al. [JMM09].

Several macro photos from a hair strand are taken with a very shallow depth of field, sweeping the plane of focus through the hair volume. The shallow depth of field reduces occlusion and isolates the visible filaments lying on the focus plane. The 3D position of the visible fibers can be computed in every frame from the known camera pose and intrinsic parameters. The results are promising, but such an approach is only suitable for the reconstruction of detached hair strands.

Wang et al. [WYZG09] proposes an approach to model a hairstyle with a statistically similar spatial arrangement of strands and geometric details of a given input hair geometry. A 2D feature map characterizing the input hairstyle is calculated and from it an output feature map is generated using texture synthesis techniques. The output hairstyle is then generated according to the information coded in the generated feature map. This technique can run completely automated, however user-controlled editing of the resultant hairstyles can be accomplished by manipulating the 2D feature map.

By nature, all methods presented so far are prone to stability issues related to global optical effects such as self-shadowing and multiple scattering. From a conceptual point of view our approach is closely related to both Wei et al. [WOQS05] and Paris et al. [PBnS04]. However, using thermal imaging most of the limitations related to those approaches –manual segmentation of the hair region, inaccurate visual hull representation of the hairstyle volume, or global illumination effects– can be avoided. This way a more robust reconstruction approach with virtually no illumination constraints is possible using a single hand-held device.

3.3 Thermal Imaging

Thermographic cameras are imaging devices that capture radiation in the far-infrared range of the electromagnetic spectrum (7500nm–14000nm), opposed to conventional cameras that capture radiation in the visible range (400nm–750nm).

According to the technology of its detector, thermal cameras can be classified broadly in two types: those using cooled quantum detectors and those

using uncooled thermal detectors. Quantum detectors are based on an inner photo-electric effect according which electrons are set free between two layers of a semi-conductor device [Nol07]. Quantum detectors are very sensitive, approaching a Noise-equivalent temperature (NET) of about 10mK. This high sensitivity allows the use of lenses with higher F-number[1], making lenses with longer focal lenses both smaller and cheaper. However, cameras based on this type of detectors require an external cooling system and the cooling process is both time and energy consuming.

Uncooled thermal detectors work under the principle that the sensor's electrical properties –resistance, voltage or current– change when heated by infrared radiation [BAF07]. These changes can be measured and transformed to intensity values. Thermal detectors are mostly based on pyroelectric materials of microbolometer technology and are less sensitive than quantum detectors, with NET values ranging from 80 mK to 200 mK. Nevertheless, they do not require any cooling system and are thus considerably less expensive than the quantum detectors.

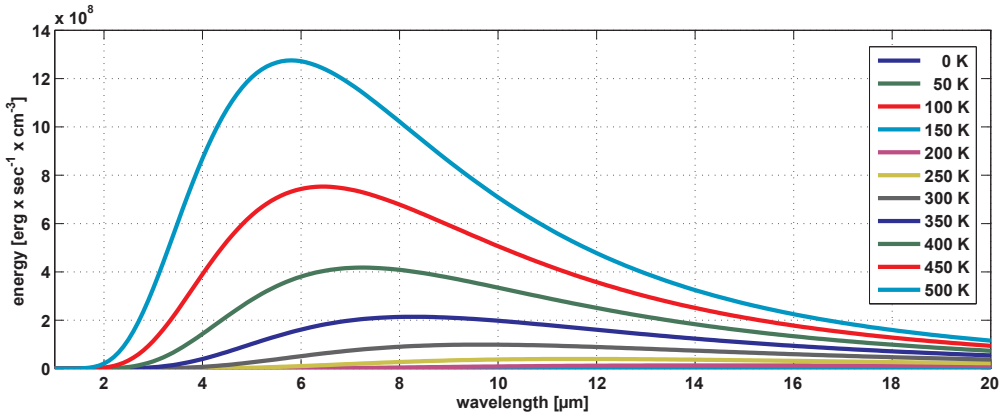

Figure 3.2: Black-body radiation curve for different temperatures. The frequency and intensity of the curve's peak increase with the temperature, implicitly meaning that more radiation.

According the black body radiation law, every object with temperature above the absolute zero emits electromagnetic radiation [DB96] (Figure 3.2).

[1]Ratio of the lens's focal length to the diameter of its entrance pupil.

The Planck Law defines the spectral emission E of an object as function of its temperature T and wavelength λ [WZ85]:

$$E(\lambda, T) = \frac{2hc^2}{\lambda^5} \frac{1}{e^{(hc/\lambda k_B T)} - 1} \tag{3.1}$$

where

$$\begin{aligned} h &= 6.625 \cdot 10^{-27} \text{ erg} \cdot \text{sec (Planck constant)} \\ k_B &= 1.38 \cdot 10^{-16} \text{ erg/K (Boltzmann constant)} \\ c &= 3 \cdot 10^{10} \text{ cm/sec (speed of light)} \end{aligned}$$

Extremals in the specific spectral distribution can be computed from the Wien's Displacement Law based on the object's temperature T:

$$\lambda_{max} = \frac{b}{T} \tag{3.2}$$

where

$$b = 2897768.5 \cdot 10^{-3} \text{ nm} \cdot \text{K (Wien's displacement constant)}$$

Modern thermal cameras equipped with an focal plane array (FPA) of microbolometers detect these peaks in the far infrared range of the electromagnetic spectrum.

3.3.1 Heat transfer through the hairstyle

In our approach the hairstyle is treated as an homogeneous medium with the head and outer environment as inner and outer boundary respectively. Due to the difference of temperature between the three different mediums –the typical temperature range of a human head is 35.5 °C to 37.5 °C [SLFW02] and in all experiments the environment temperature was kept well below 20 °C– heat transfer takes place between the head and the environment through the hair.

During this process the heat isotropically emitted by the head is absorbed by the hair filaments. Hair fibers are primarily composed by keratin proteins

with high emissivity in the infrared range [LS83, PRO+02], hence the fraction of reflected radiation can be neglected. Assuming a state of thermal equilibrium the temperature of the hairstyle remains constant during the data acquisition, meaning that the filaments re-emit all incoming thermal radiation. The temperature distribution captured by the thermal camera represents the amount of irradiated energy that reaches the boundary of the hairstyle volume.

The nearly isotropic way that heat is transported through the hairstyle constitutes a major advantage of thermal-based modeling techniques over their conventional image-based counterparts as complicated hair reflectance, such as directional highlights and multiple scattering, can be avoided. Moreover, the temperature of hair strands locally hints about its distance to the head. Consequently, discontinuities in the temperature distribution indicate spatial discontinuities along the hairstyle boundary.

3.4 Overview

Our pipeline takes as input a video stream of thermal images from a hairstyle and generates a hair geometry reproducing the original hairstyle (Figure 3.3). It has five main stages:

- **Camera registration:** The extrinsic camera parameters are calculated using a sparse bundle adjustment approach.

- **Hair region segmentation:** The hair region is extracted from the input images. The resulting silhouettes are then used for roughly approximating the hair volume by its visual hull.

- **Hairstyle boundary reconstruction:** The hair volume gets refined by identifying voxels belonging to the boundary of the hairstyle using photo-consistency. The local relationship between temperature and distance to the head is used to further accelerate the reconstruction process by one order of magnitude.

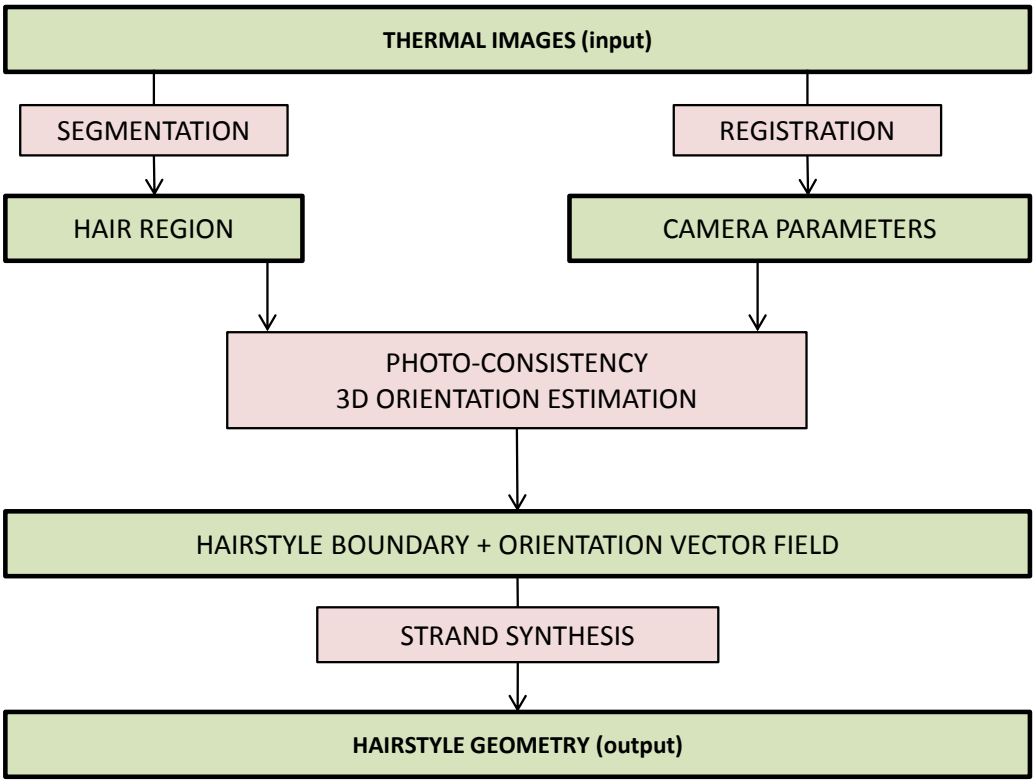

Figure 3.3: Diagram showing the different stages of our thermal-based reconstruction pipeline.

- **Hairstyle boundary characterization:** Both an orientation vector field and a temperature scalar field are generated along the surface of the hairstyle. Local image orientation used to compute the orientation field is obtained through multi-scale analysis for orientation on the thermograms.

- **Hair strands generation:** Strands are synthesized starting at surface voxels and follow the orientation field. A second step refines the shape of the synthesized hair geometry employing smoothness and curvature constraints.

3.4.1 Camera Registration

The camera pose of the thermal images is estimated using a bundle adjustment technique [SSS08]. Given a set of uncalibrated images depicting an object from different viewpoints (Figure 3.4), bundle adjustment techniques simultaneously compute the 3D coordinates of the scene geometry as well as the pose of the cameras employed to acquire the images (Figure 3.5) by minimizing the reprojection error between the locations of observed and predicted image points [TMHF00]. This error can also be used to measure the accuracy of the registration process.

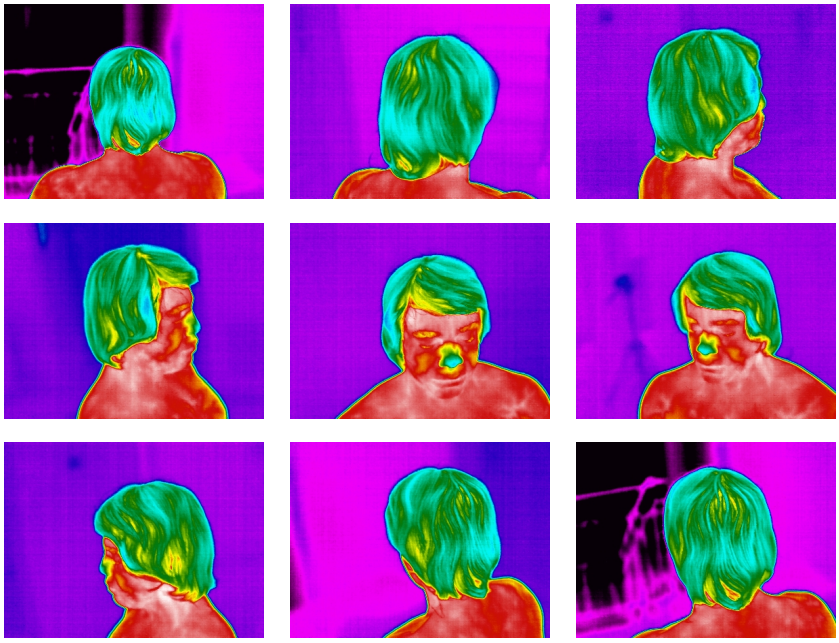

Figure 3.4: Several frames of the input sequence depicting the captured hairstyle from different angles.

As the heat is emitted isotropically from the hairstyle, the captured temperature values are nearly independent of the viewpoint. Therefore, local features are preserved across different frames while highlights and other direction-dependent optical effects that may affect the calibration are avoided.

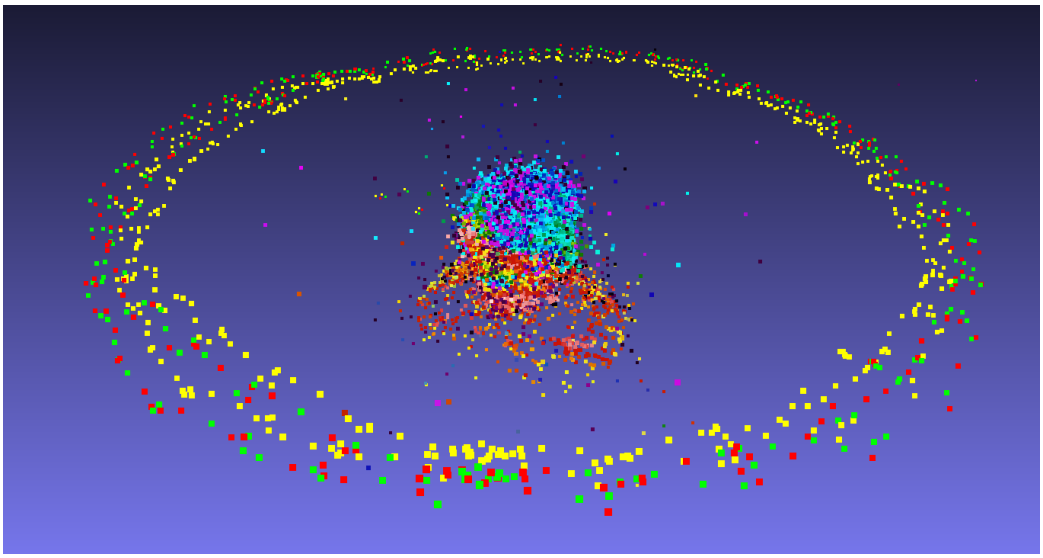

Figure 3.5: Results of the camera registration process following the approach proposed by Snavely et al [SSS08]. Points around the sparse head mesh denote the estimated position and orientation of the cameras.

3.4.2 Hair Region Segmentation

The extraction of the hair region from the thermal images is a very important step in our approach, as an accurate representation of the hair region is required for the successful estimation and characterization of the hairstyle volume. This can be a very challenging task for acquisition setups using images taken in the visual range, especially if using low resolution images, therefore to date all image-based approaches rely on some degree of interaction to accomplish this task.

In our approach the hair region is extracted in a simple, automated and very accurate way, using the temperature values directly. As the skin temperature on humans lies over 35 °C [SLFW02] and the room temperature was kept at 17 °C during data acquisition, areas in the image can be classified as background, skin and hair regions using simple thresholding (Figure 3.6). The hair region was assumed to be in the range of 20 °C to 30 °C for all our examples. A Level Set Method (LSM)-like shape recovering technique [MS98] helps to regularize the computed silhouettes and eliminate spurious texels in the resultant binary images (Figure 3.7).

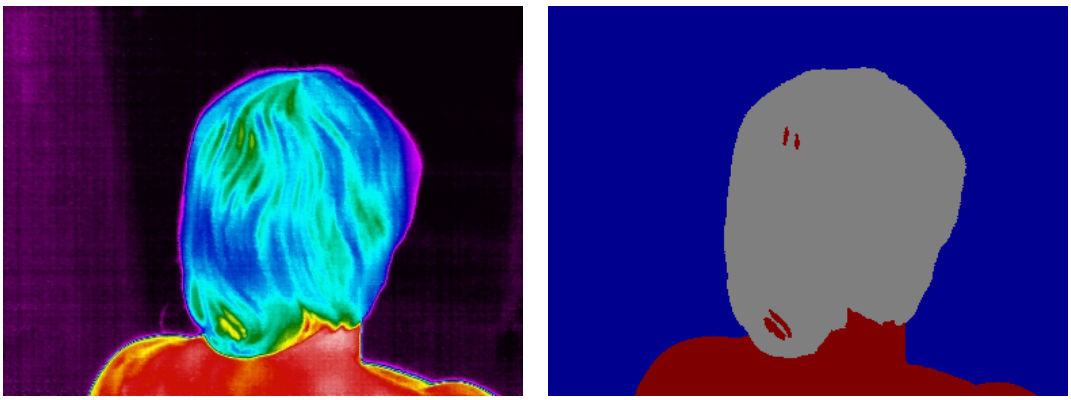

Figure 3.6: The hair region (gray area on the right image) is easily extracted from the thermal images (left image) using two predefined temperature thresholds.

Figure 3.7: Extracted foreground from the input sequence using our threshold-based approach.

3.4.3 Hairstyle Boundary Reconstruction

The next step of our approach involves the reconstruction of the hairstyle volume, using the estimated parameters of the cameras employed to acquire the thermal images as well as the extracted hair regions. This step is a cornerstone of our approach, since the generation of the hair geometry – our ultimate goal– is based on information extracted from the input data and projected over the reconstructed volume. More precisely, to reconstruct the hairstyle volume we estimate its boundary, a set of voxels resembling

the surface which is computed by means of photo-consistency [SD97]. Since the captured temperatures are nearly viewpoint independent, a consistency measure based on temperature works exceptionally well.

To improve its performance, the reconstruction process is divided in four steps:

- A visual hull of the model is computed using the extracted hair regions and the camera parameters.
- The hairstyle boundary is coarsely approximated by computing the depth of a sparse set of image samples using conventional photo-consistency assuming that the actual surface is bounded by the visual hull.
- The hair regions are densely sampled with sub-pixel accuracy and their depth is computed taking advantage of a local relationship between temperature and distance to the head. Thanks to this relationship the surface region is restricted to a thin layer based on the position of the sparse sampling. Considering only depths within this layer the efficiency of the photo-consistency is increased by one order of magnitude.
- The shape of the resultant surface is improved considering photo-consistency and monotony between temperature and distance to the camera among neighboring samples.

Visual Hull as initial approximation of the hairstyle volume. The visual hull [Lau94] is a geometric approximation of an object computed from projected silhouettes. Its computation is very fast, but by definition it cannot represent concavities and fails to capture complex geometric features, such as curls (Figure 3.8). However, we compute the visual hull as a bounding volume for the hair that is used to speedup subsequent reconstruction steps.

Refining the hairstyle volume using photo-consistency. A voxel is considered to be *photo-consistent* if its temperature appears to be similar

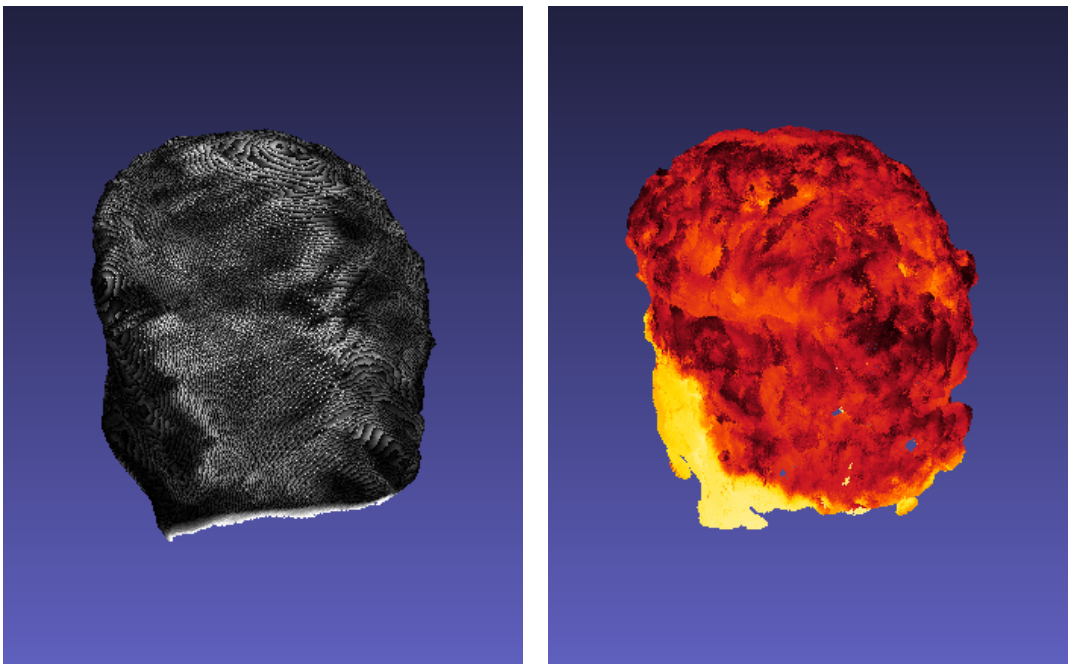

Figure 3.8: Comparison between a model's visual hull and the reconstructed surface, color coded according to its temperature.

to all cameras that can see it. Using photo-consistency as a measure we decide whether a voxel inside the visual hull volume belongs to the hairstyle boundary or not.

The basic idea is to compute photo-consistency along camera rays inside the boundaries of the visual hull, where a maximum indicates an intersection with the hairstyle's surface. Reconstruction based on thermal images is particularly reliable, since the projections of surface voxels are free of directional artifacts because heat is emitted nearly isotropically.

Visibility is a critical factor influencing photo-consistency. Since in our approach no visibility information of voxels is available, we base on the method proposed by Vogiatzis et al.[VHETC07] that does not require any explicit visibility information.

The major drawback of this method is its computational cost, caused by the high number of considered cameras and the amount of samples required to faithfully reconstruct the hairstyle surface. We avoid this bottleneck by

analyzing the temperature distribution over the hair region.

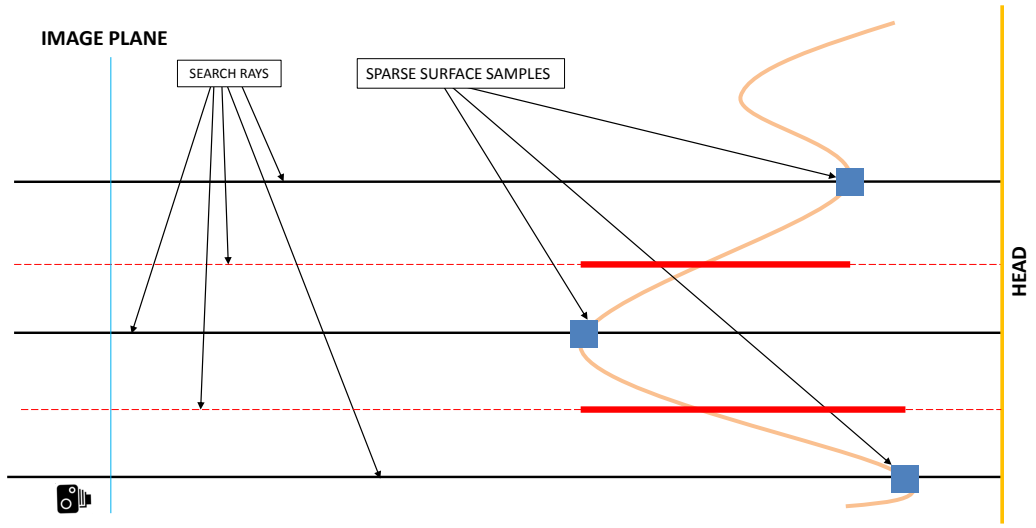

Figure 3.9: How the accelerated photo-consistency works. The search interval (bold red segment) for intersection with the surface along the camera ray (dotted red line) of the dense samples is constrained by the depths of the sparse samples (blue dots).

Accelerating photo-consistency. A coarse approximation of the hairstyle boundary is obtained by computing the depth of a sparse set of image samples using conventional photo-consistency. A finer boundary approximation is estimated by densely sampling the hair regions with sub-pixel accuracy. The depths of these samples are efficiently computed based on the sparse samples and using a heuristic that correlates temperature and distance to the camera of points at the hairstyle boundary (Figure 3.9).

This heuristic is based on the assumption that –locally– warmer points are nearer to the head than colder ones, motivated by the idea that for neighboring boundary points the difference in heat transport and thus temperature is dominated by the distance to the head. This means that for small boundary patches located between the head (heat source) and the camera a similar relationship can be expected for the camera: the lower the temperature the closer to the camera.

To estimate the depth of the dense samples a 3D kD-tree is built, in-

corporating both 2D position in image space and temperature of the sparse samples. Using this information we process the dense samples as follows:

- A knn search is performed for each dense sample with temperature t_s to retrieve its nearest neighbors.

- Let d_{min} and d_{max} be the depth values of the sparse samples with minimum (t_{min}) and maximum (t_{max}) temperature among the retrieved neighbors. Depth is computed using conventional photo-consistency along the interval $[d_{min}, d_{max}]$ if $t_{min} \leq t_s \leq t_{max}$, otherwise only one of the interval bounds is valid, depending on whether $t_s < t_{min}$ or $t_s > t_{max}$.

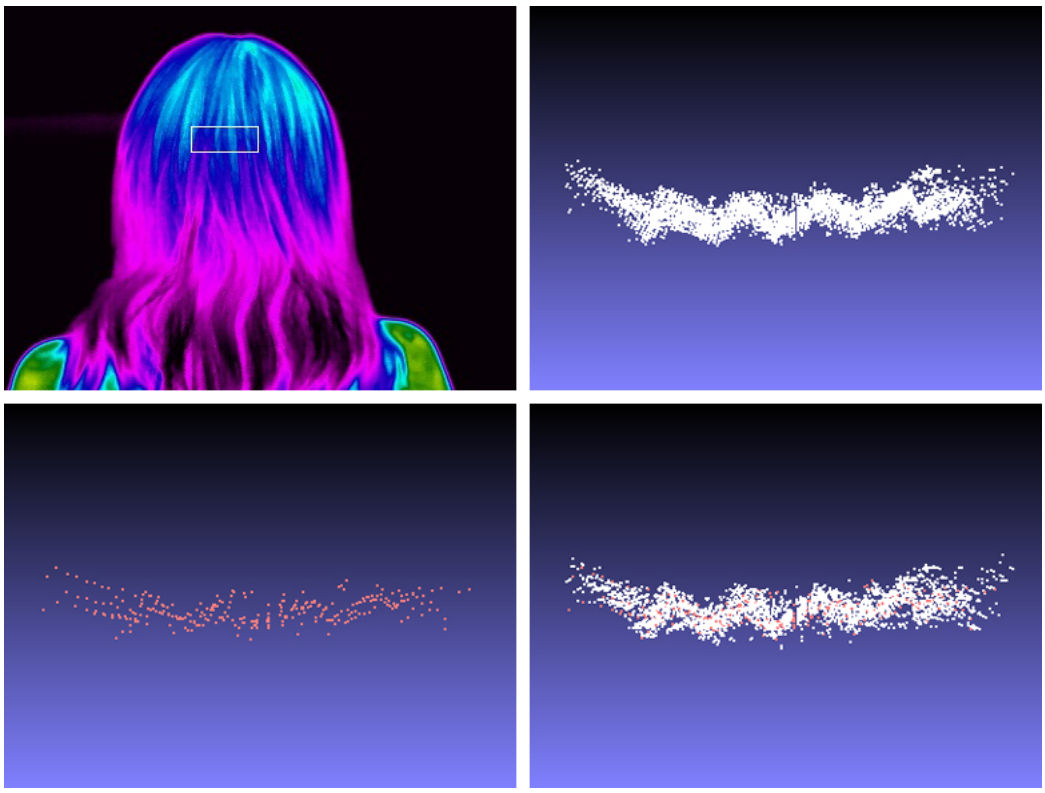

Figure 3.10: A surface patch (white rectangle at left top image) reconstructed using conventional photo-consistency (right top image) and by our accelerated approach (right bottom image) based on sparse sampling (left bottom image).

The described process is based on the local monotony of distance with respect to temperature. Strictly speaking, this monotony holds only for samples near the center of projection, if the viewing direction is aligned with the normal of the heat emitting surface. However, depth tends to vary very rapidly in convex areas near the silhouette, meaning that the computed intervals are less tight. In addition, the search intervals are not bounded at all if the monotonicity condition is not satisfied. This simple heuristic reduces considerably the computational cost of the reconstruction process and accelerates it in more than one order of magnitude (Figure 3.10).

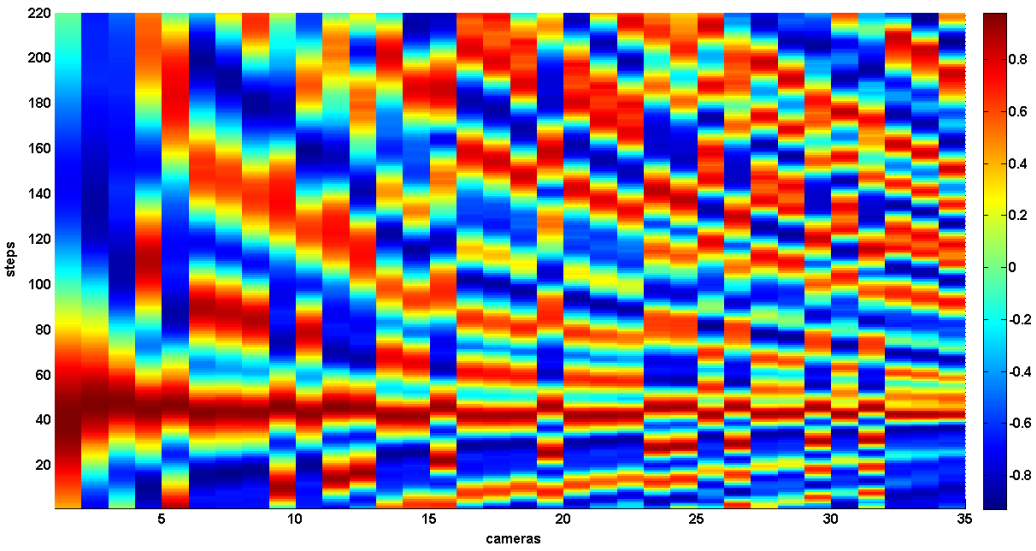

Figure 3.11: Depth estimation of an image sample. The intersection of the sample ray with the hairstyle boundary is computed based on normalized cross-correlation (NCC) between the image sample and the projection of discrete steps along the ray on neighboring cameras. In the example shown the boundary is located between steps 40 and 50.

Improving the hairstyle surface A final refining step is performed to further improve the reconstructed surface. Due to the rather low resolution of the thermal images, the dense sampling during surface reconstruction and the small distance between the cameras considered in our pipeline, the depth of some image samples cannot be accurately computed. In such cases there is

no clear peak among the photo-consistency values around the actual hairstyle boundary (Figure 3.11).

Since, according to our consistency-based measure, the surface intersection could be anywhere along this *uncertainty interval* we base on the monotony of distance with respect to temperature to accurately locate it. More precisely, an optimization process estimates the sample's depth considering photo-consistency and local temperature-distance-monotony. Let s_i be an image sample with computed depth d_i, temperature t_i, photo-consistency $\phi(s_\mathrm{i})$ and $N(s_\mathrm{i})$ be the set of neighboring samples in a fixed-size neighborhood. The exact depth $\mathbf{d^i}_{opt}$ is computed according to the function

$$\mathbf{d^i}_{opt} = \underset{\mathbf{d_i}}{\operatorname{argmin}}(\exp(-\mu \cdot \phi(s_\mathrm{i})) + \sum_{j \in N(s_\mathrm{i})} (\neg((d_\mathrm{i} \leq d_\mathrm{j}) \wedge (t_\mathrm{i} \leq t_\mathrm{j})))) \qquad (3.3)$$

where $\mu = 0.5$ is a constant decay factor. The first term of the function accounts for the photo-consistency of the sample whereas the second term controls the temperature-distance relationship between the sample and its neighbors, evaluating to zero if the monotony condition is fulfilled.

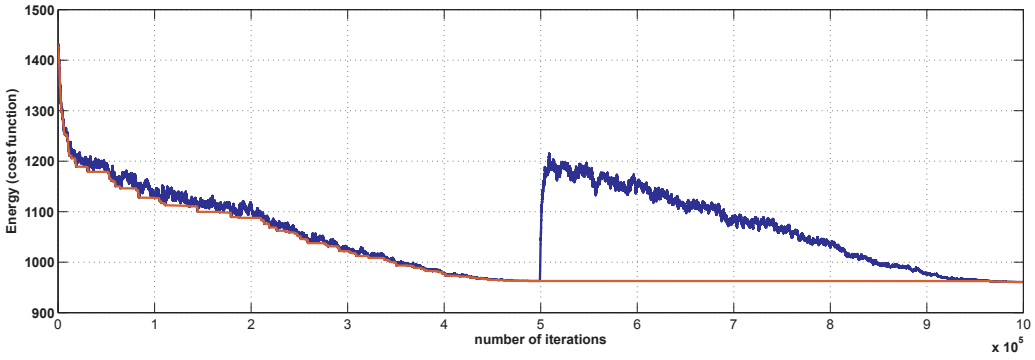

Figure 3.12: Evaluation of the cost function (Eq. 3.3) as a function of the number of iterations during monotony-based optimization for a surface patch. The blue line indicates the energy of the computed displacement configurations (states) whereas the red line shows the energy of the accepted states.

During optimization only depth values within the sample's uncertainty interval are considered. Since these depths represent discrete steps along the sample's image ray, the minimization of equation 3.3 can be treated as a

typical combinatorial problem. Since an exhaustive evaluation of all possible combination is unfeasible, we compute the optimum sample's depth values by means of a *simulated annealing* approach [BT93] (Figure 3.12).

After performing this process for each of the cameras a volumetric representation of the hairstyle is obtained (Figure 3.13).

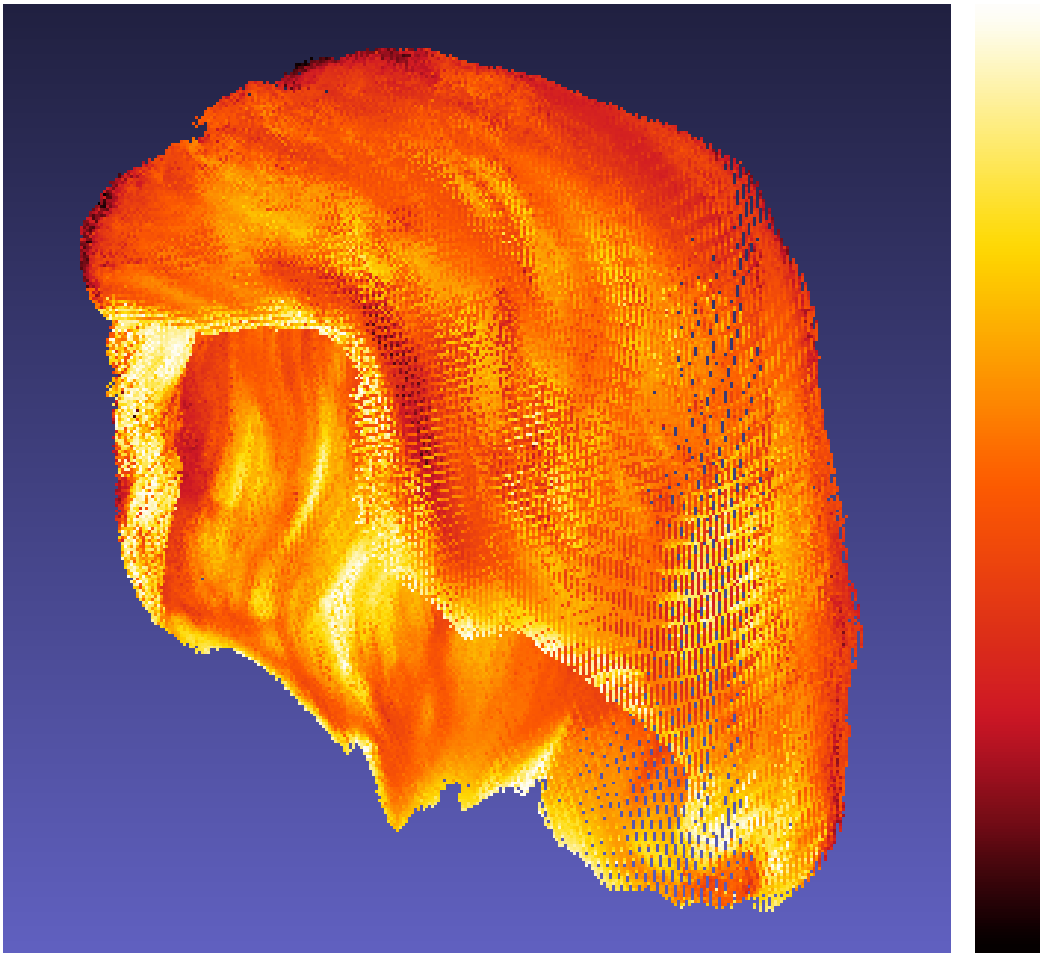

Figure 3.13: Reconstructed hairstyle boundary, color coded according to its temperature.

3.4.4 Hairstyle Boundary Characterization

Information regarding location, length and orientation of the hair filaments within the hairstyle boundary is required for the successfully generation of hair geometry inside the reconstructed volume. Since the synthesized geometry should resemble the captured hairstyle the necessary information is extracted from the input thermal images and projected onto the hairstyle volume boundary.

Since our hair geometry synthesis is based on temperature and spatial orientation, temperature and image orientation information are extracted from the input thermograms and combined to generate a temperature scalar field and an orientation vector field along the hairstyle surface. More specifically, surface voxels are back-projected to the images considering occlusion using the visibility information obtained during reconstruction of the hair surface. The temperature on the voxels is computed by averaging the projection values on the thermal images and its local spatial orientation is estimated based on the local image orientation at the projections.

Calculating the image orientation. The local orientation of the thermal images is calculated using *steerable filters* [Fre92]. A steerable filter is defined by a convolution kernel K synthesized as a linear combination of a set of basis filters that can be rotated arbitrarily. Let I be the image being analyzed, the convolution of K_θ –K rotated by an angle θ– with I at (x, y) produces a score $F(\theta)$. The predominant orientation $\bar{\theta}$ at (x, y) is then $\bar{\theta} = \text{argmax}(F(\theta))$ and the corresponding score $F(\bar{\theta})$ is taken as the pixel's orientation strength.

The image orientation extraction is performed in a multi-scale fashion to improve the robustness of the collected data (Figure 3.14). The image is smoothed several times using a *Gaussian Smoothing Filter* with increasing kernel size and the results of this operation are stored as layers of a tensor of order 3. Orientation information is then extracted from each one of the layers, meaning that for every image pixel a vector of 2D structures storing predominant orientation and strength is obtained. The structure with the maximum orientation strength along the vector is selected as the local ori-

entation of the pixel. This multi-scale approach assures that the resultant orientation information is not influenced by high frequency, nonrepresentative structures that may be present in the image.

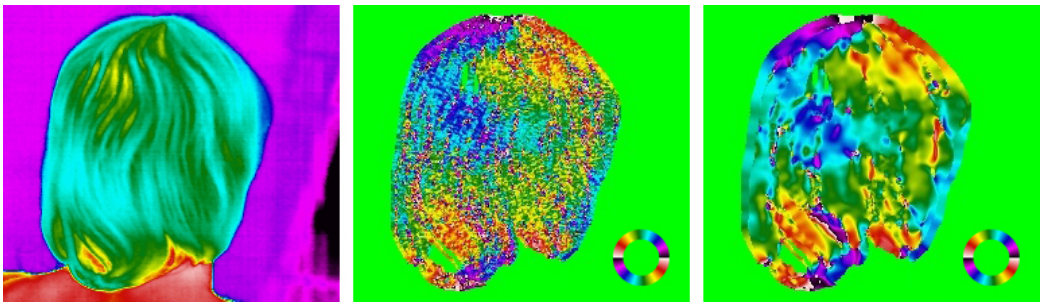

Figure 3.14: Results of the orientation analysis. From left to right: original thermogram, response of the orientation filter applied to the hair region and combination of the responses of the orientation filter at different scales.

Triangulating orientation. As already mentioned, the orientation vector field on the surface of the hairstyle is computed by projecting the surface voxels on the images where they are visible and combining the local orientation information at their projections. More precisely, the voxel's spatial orientation is computed by solving a linear equation system in least square sense like done by Wei et al. [WOQS05], as it has to be consistent with their projections.

Let v be a surface voxel with spatial orientation $\vec{d}_{\mathrm{v}}$ and $vis(v)$ the set of images where v is visible. For each image I_i where $I_i \in vis(v)$ we have two equations:

$$\vec{d}_{\mathrm{v}} \cdot \vec{n}_{\mathrm{i}} = 0 \tag{3.4a}$$

$$\vec{d}_{\mathrm{v}} \cdot \vec{n}_{\mathrm{v,i}} = 0 \tag{3.4b}$$

where $\vec{n}_{\mathrm{i}}$ is the normal of the image plane and $\vec{n}_{\mathrm{v,i}}$ is the normal of the plane spawned by $\vec{n}_{\mathrm{i}}$ and the backprojection of v's image orientation on I_i's image plane.

The spatial orientation $\vec{d}_{\mathrm{v}}$ is estimated by minimizing the function

$$\sum_{I_i \in vis(v)} ((\vec{d}_{\mathrm{v}} \cdot \vec{n}_{\mathrm{i}})^2 + (\vec{d}_{\mathrm{v}} \cdot \vec{n}_{\mathrm{v,i}})^2), \text{ subject to } \|\vec{d}_{\mathrm{v}}\| = 1 \tag{3.5}$$

whose solution is the vector associated to the smallest singular value of the coefficient matrix related to the equation system (Figure 3.15 right).

The inverse of the error between the projection of the estimated 3D orientation and the original image orientation is used to measure the reliability (r_{v}) of the estimation (Figure 3.15 left). This measure will be used in the subsequent synthesis of hair strands.

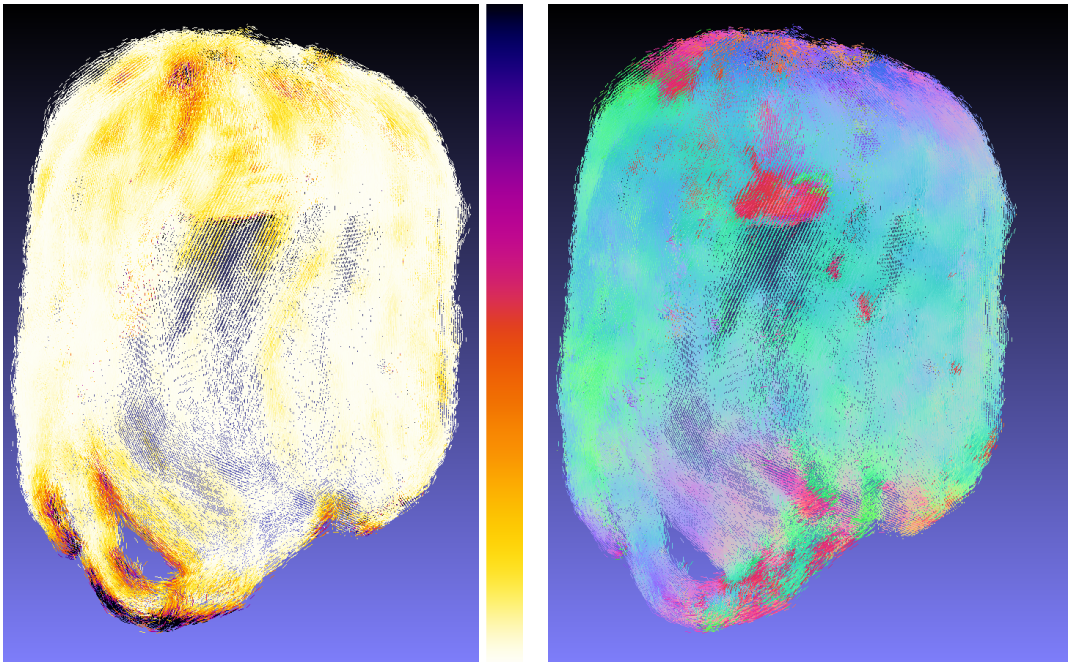

Figure 3.15: Resultant volumetric orientation field. The spatial orientations are color coded according to r_{v} (left image) and spatial angle (right image).

3.4.5 Hair Strands Synthesis

The final step of the reconstruction pipeline involves the generation of the hair strands. In contrast to prior approaches who start growing at the scalp

[PBnS04, WOQS05, PCK+08, WYZG09], filaments start to grow in the most reliable regions of the boundary –characterized by r_v– and follow the orientation vector field as long as consistent orientation and temperature information is available. Subsequently the shape of the filaments is refined to improve its appearance and finally hair segments are joined at loose ends.

Growing the filaments along the surface. The filaments grow by taking N evenly distributed samples on the boundary of the hairstyle as "seed" voxels. Starting at the seeds a strand segment is formed by bidirectional explicit numerical integration along the orientation field similar to [PBnS04, WOQS05, PCK+08]. However, using local filtering of orientations preferring smooth temperature gradients and high orientation reliability r_v help to guide the synthesis by reducing the weight of implausible data. Let p_{end} be the position of the filament's end v_{end} and $N(p_{end})$ be the list of the neighboring voxels. The direction $\vec{d}_{new}$ of the new segment computes as:

$$\vec{d}_{new} = \sum_{v \in N(p_{end})} w_v \cdot \vec{d}_v \tag{3.6}$$

The weights w are computed based on the position of the neighbors p_v, its temperature t_v and orientation reliability r_v as follows:

$$w_v \sim \left(\frac{1}{|p_{end} - p_v|} \cdot \frac{1}{|t_{end} - t_v|} \cdot r_v\right) \tag{3.7}$$

The position p_{new} of the new filament vertex v_{new} is computed based on $\vec{d}_{new}$ through explicit numerical integration.

A filament grows as long as the new generated vertex lies on the boundary of the hairstyle and its orientation and temperature are consistent with the orientation and temperature at the filament's end. More precisely, let δ_{dst}, δ_{tmp} and δ_{dir} be distance, temperature and orientation thresholds. The filament's growth phase stops if at least one of the following conditions is not satisfied:

- $|p_{new} - p_{near}| < \delta_{dst}$ where p_{near} is the position of the nearest boundary

voxel.

- $\frac{\vec{d}_{\text{new}}}{|\vec{d}_{\text{new}}|} \cdot \frac{\Omega(p_{\text{new}})}{|\Omega(p_{\text{new}})|} < \delta_{\text{dir}}$ where $\Omega(p_{\text{new}})$ is the orientation field evaluated at p_{new}.

- $|t_{\text{new}} - t_{\text{end}}| < \delta_{\text{tmp}}$ where t_{new} and t_{end} are the temperatures at v_{new} and v_{end} respectively.

To check whether a vertex is valid or not we first consider a $5 \times 5 \times 5$ around the respective voxel. If no surface voxel is found we assume v_{new} to lie outside of the hair volume and stop integration. Accordingly, we choose $\delta_{\text{dst}} = 2.5 \cdot \Lambda$ where Λ is the extent of a voxel.

Moreover, we stop growing if temperature or orientation vary rapidly, to avoid growth across depth and orientation discontinuities. Considering typical temperature and orientation variation for adjacent pixels along a strand we set $\delta_{\text{tmp}} = 1\text{K}$ and $\delta_{\text{dir}} = \cos(10°)$. In a subsequent step we attempt to join the created filament segments at their end points. This is especially useful to "bridge gaps" where wisps cross.

Finally, each filament F_i is converted to a cubic spline representation computed from a set of control points $\mathbf{x^i} = x_j^i$ obtained by sub-sampling every 16-th vertex of the filament curve. This gives a compressed, analytical and smooth representation of the filament, used for subsequent curvature-based regularization.

Regularization using curvature constraints. Due to the image-based nature of our hair volume characterization technique (see section 3.4.4) spatial orientation is computed only for visible boundary voxels. This means that important information regarding the hair topology in areas inside the volume not directly visible to the cameras is missing. The absence of orientation information inside the hairstyle is a serious limitation as occluded filament sections cannot be reconstructed. This limitation is critical when modeling curly hair, where strands are quite frequently occluded by other strands and the –along the hairstyle boundary– estimated orientation field sometimes does not accurately reproduces the shape of the filament. The

latter leads to hair strands having a rather unrealistic appearance despite faithfully following the orientation field.

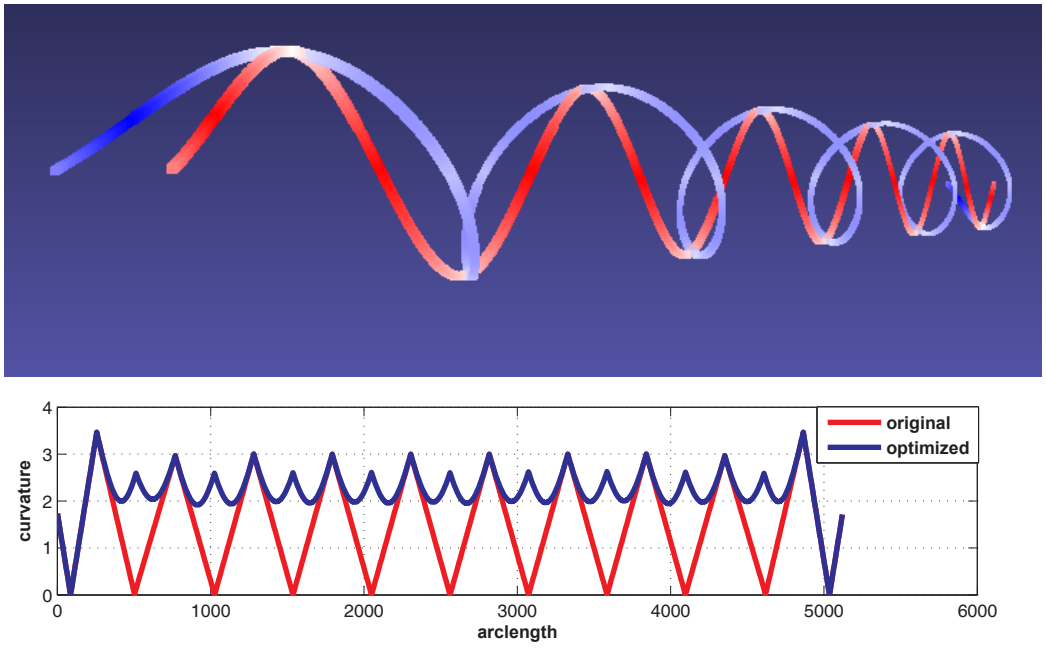

Figure 3.16: Performing curvature-based regularization on a spatial curve. Top: perspective view of a sinusoid (red line) and the resulting helix (blue line) after curvature-based regularization. Bottom: Plot of curvature vs. arclength before and after optimization.

To solve this problem and improve the appearance of the synthesized hair strands we take advantage of model-based regularization. According to [BAC+06] the equilibrium shape of hair filaments can be well approximated by piecewise helical rods. Since using a physically-based model directly on a per filament basis is not practical we make the simplifying assumption that the curvature remains constant along the filament segments. According to that we attempt to minimize variations of the curvature along the filament while at the same time matching orientation and temperature values available at the hairstyle boundary.

Let p_j^i be the position and T_j^i, κ_j^i the analytically computed tangent and curvature values at the control points x_j^i of the spline representing the i-th filament. The shape of the filament is then refined by "sliding" x_j^i along the

viewing ray of a reference camera according to:

$$\mathbf{z^i}_{\text{best}} = \underset{\mathbf{z^i}}{\text{argmin}}(\sum_{j=1}^{N}(\frac{\partial \kappa_j^i}{\partial_j} + \sin(\arccos(\frac{T_j^i}{|T_j^i|} \cdot \frac{\Omega(\bar{p_j^i})}{|\Omega(\bar{p_j^i})|}))) \tag{3.8}$$

where z_j^i denotes the depth of x_j^i along the camera's viewing ray and $\bar{p_j^i}$ is the projection of p_j^i on Ω.

The first term of the function represents the derivative of the filament's curvature whereas the second term accounts for the angle between the tangent of the filament and the computed orientation vector field. The reference camera is selected among the cameras where x_j^i is visible as the one in which the distance between the imaged x_j^i and its principal point is minimal.

The optimization problem described by equation 3.8 is solved with the help of a conjugate directions method [Pow64], perfectly suited since the partial derivatives of our objective function cannot be computed analytically. Figure 3.16 shows the results of the regularization on a synthesized filament whose projection is a sinusoid whereas in Figure 3.17 the results of the process in a synthesized hairstyle can be seen. While before optimization (3.17 left) the generated filaments show some degree of clumpiness and lack of depth, after optimization (3.17 right) these artifacts are corrected in a great extent.

Joining loose ends and connecting the filaments to the scalp. During strand generation the growth phase of certain segments was aborted due to the consistency constraints. However, some of these segments may be part of longer hair strands having ambiguities along the orientation paths, e.g. hair crossings. To solve this issue we build a 6D kD-tree with position and orientation of all filament ends and attempt to connect the loose ends as follows:

- A knn search is performed for every segment end e according to its position p_e and orientation d_e.

- For each retrieved neighbor e_i an interpolation spline connecting it with e is computed. Let κ_i be the spline's average curvature, we keep $\kappa_{\text{min}} =$

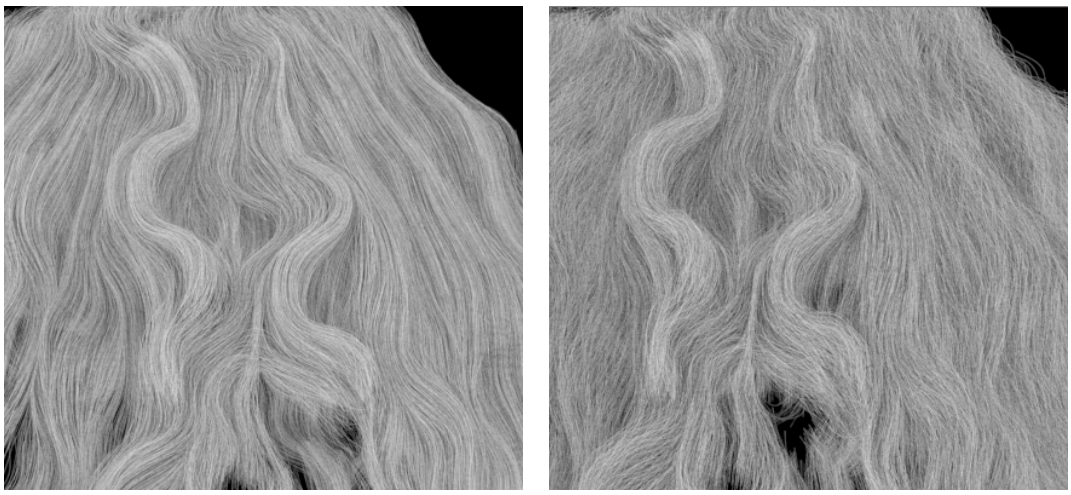

Figure 3.17: Effect of curvature-based regularization on a wavy hairstyle. Lack of depth and clumpiness present before regularization (left image) are corrected in the resultant geometry (righ image).

$\min(\kappa_i)$ and $e_{\text{opt}} = \text{argmin}_{e_i}(\kappa_i)$ as the candidate to be connected with e.

- The segments are joined only if $\kappa_{\min} < \min(\kappa_e, \kappa_{\text{opt}})$, where κ_e and κ_{opt} are the average curvatures of the segments containing e and e_{opt} (Figure 3.18).

Following this procedure only segments with smooth connection curves are joined.

A cubic spline representing the new filament is computed for every pair of connected segments and the end's combination is removed from the list of potential connections to avoid repetitions. After finishing the process, filaments whose length lies outside two standards deviations of the average length are considered as loose segments and removed from the hair geometry.

Finally, the resultant filaments are connected to a user-defined ellipsoid approximating the head. To that end, we compute a spline connecting the filament's end with the centroid of the ellipsoid.

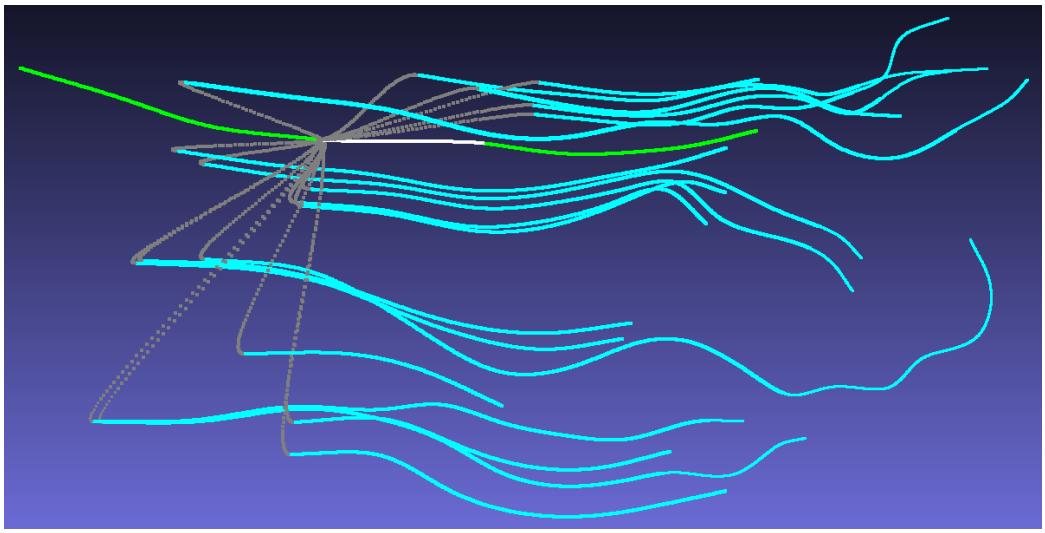

Figure 3.18: Segments are joined by a connecting interpolation spline. The optimum connection (white line) is selected among the splines (grey lines) linking a given segment (green line) with its neighbors (cyan lines) considering curvature. The two linked segments form a new filament.

3.5 Discussion and Results

To test the effectiveness of our approach different hairstyles –varying in hair length and degree of curliness– have been reconstructed (Figure 3.19). The rather low resolution of the thermal camera (384 × 288 pixels) prevents us from obtaining information at filament level. Nevertheless, geometrical features generate distinctive temperature variations which are faithfully captured by the thermal cameras, even if they are hardly, if at all, visible –due to shadowing or poor lighting– when using conventional imaging techniques. The comparison given in row 1 and 2 of Figure 3.19 illustrates that thermal images are better suited to reveal characteristic geometrical features than conventional images.

The input data was captured with a VarioCAM© thermal camera (Figure 3.20) and all hairstyles were reconstructed using a Core i5 @2.6 GHz CPU arquitecture. Average run-times for the different stages of our method (reconstruction from 300 images, generation of 100000 filaments) are given in Table 3.1. Moreover, Table 3.2 shows some statistical information extracted

from the synthesized hair geometries.

Surface Reconstruction		**Filament Generation**	
Sparse	Dense	Generation	Regularization
50 min.	50 min.	12 min.	60 min.

Table 3.1: Average runtimes of the different stages of our pipeline for a hairstyle with 100000 filaments, reconstructed from 300 images. Please note that surfaces are reconstructed based on 1000 sparse samples (column 1) and 10000 dense samples (column 2) per image respectively.

Hairstyle	**Length**	**Curvature**
long straight	105	0.0048
short curly	35	0.0088
short straight	66	0.0031

Table 3.2: Average length and curvature of the generated hairstyles, computed from the spline representation of the filaments.

Along the different stages of our approach several issues had to faced:

Geometric camera calibration The simplicity of our hand-held-based acquisition step is one of the assets of our approach. Nevertheless, since the pose of the cameras is approximated using a *structure from motion* technique, an analysis of the re-projection error is imperative. By taking this error as a measure of the camera pose's reliability we counter the negative effect of working with approximated camera positions opposed to more complex, calibrated data acquisition setups.

Hair region segmentation Although the segmentation based on temperature is fast and extremely simple in general, there are still challenges that need to be taken into consideration when using our method:

- For hairstyles having a large volume the boundary is often hardly visible due to little temperature differences with the background. In such cases more images and a lower room temperature is required to obtain reliable results.

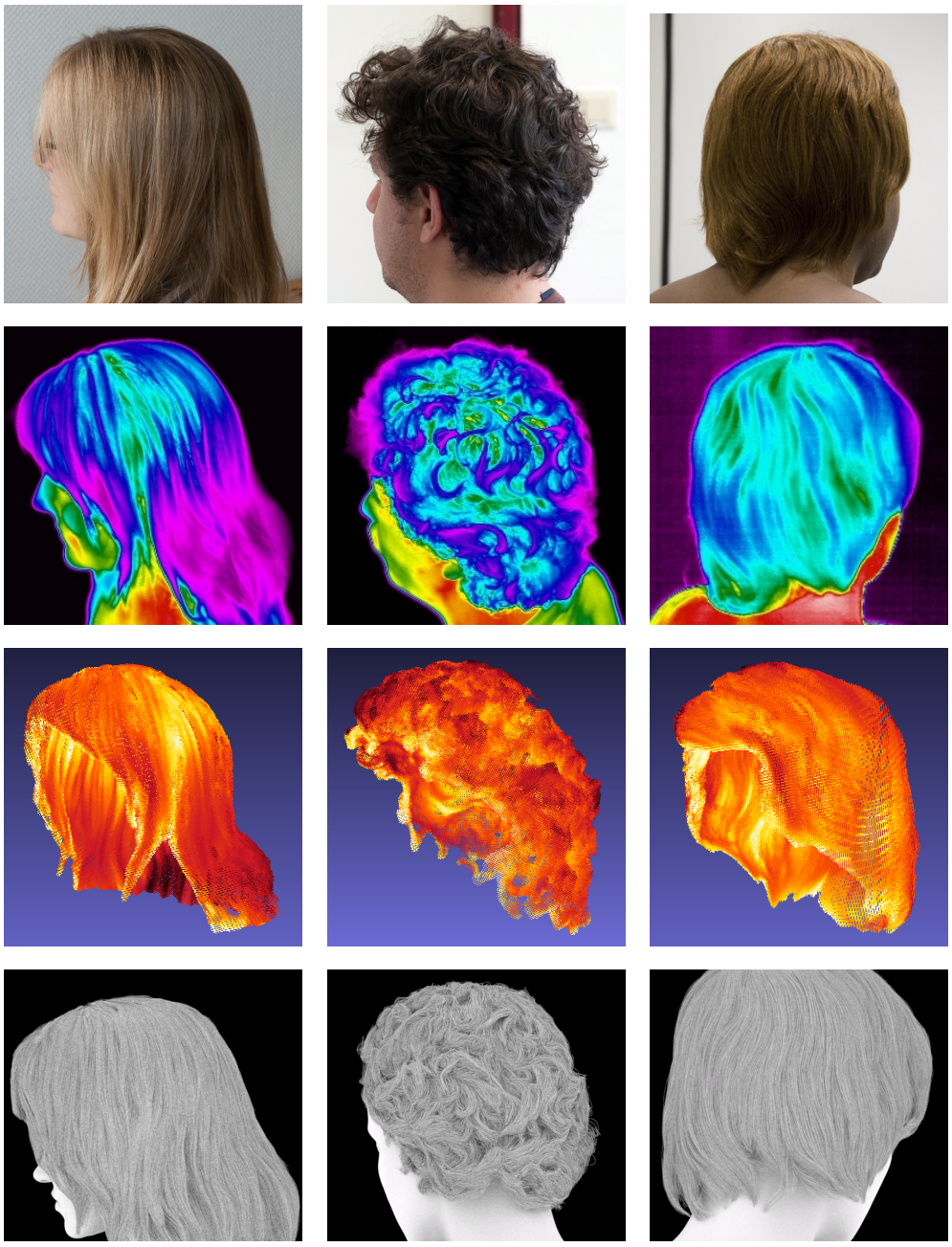

Figure 3.19: Results of our hairstyle reconstruction approach. In the first and second rows conventional and thermal pictures of our models can be seen. The third and fourth rows show the reconstructed hairstyle boundaries and the generated hair geometries rendered with ambient occlusion.

- Occasionally, facial areas that exhibit a lower surface temperature – such as the nose– are treated as part of the hair region. In this case the boundary reconstruction step is likely to generate more than one connected component. Simply considering only the biggest connected component has proven to be quite effective for all hairstyles.

Figure 3.20: Thermal camera VarioCAM© hr Research used for data acquisition.

Hair volume reconstruction The performance of image-based reconstruction approaches is strongly influenced by the (lack of) visibility information, since this plays an essential role in the triangulation of the object boundary. In order to compute the visibility information we attempted to track pixels belonging to the hair region along the threrograms using a technique based on *optical flow* [FW06]. However in regions of low contrast no precise pixel translation could be computed between consecutive images. The large aperture of the attached lens results in a very shallow depth of field, and due to the convexity of the human head large areas of the hairstyle lie outside the depth of field and appear blurred in the image. Therefore no consistent visibility information could be generated based on pixel tracking, leading us us to follow the idea presented by Vogiatzis et al. [VHETC07] in which no visibility information is required.

The accuracy of the accelerated photo-consistency could be improved using a dynamic approach. A Delaunay triangulation Λ is computed for the sparse image samples. The dense samples are then processed as follows:

- A search is performed in Λ for each dense sample s with temperature t_s to find the containing triangle Δ_s.
- Let $d_{\min}$ and $d_{\max}$ be the depth values of the Δ_s's vertices with minimum ($t_{\min}$) and maximum ($t_{\max}$) temperature. Depth is computed using conventional photo-consistency along the interval $[d_{\min}, d_{\max}]$ if $t_{\min} \leq t_{\mathrm{s}} \leq t_{\max}$, otherwise only one of the interval bounds is valid, depending whether $t_{\mathrm{s}} < t_{\min}$ or $t_{\mathrm{s}} > t_{\max}$ (Figure 3.9).
- s is added to Λ.

The main advantage against our technique lies on the constant refinement of Λ. However, computing a triangulation for a constantly increasing point set regularly is too costly to outperform our original approach.

Hair strands generation The main goal of the filament regularization step is to improve its visual appearance while remaining consistent with the orientation vector field. To achieve this the valid positions of the filament control points are constrained to lie along a "slide direction", computed according to the location of the cameras in which the control point is visible.

Different approaches to determine the slide direction were tested, ranging from combining the point's lines of sight of the visible cameras to selecting a reference camera for the whole filament and setting as slide direction the corresponding lines of sight. The best results were obtained by setting for each control point as slide direction the line of sight of the most central camera, where this "centrality" is measured as the distance between the the image projection of the control point and the image's central point.

Some other issues can be seen in the final renderings (Figure 3.21): Hair models may suffer from unrealistic "clumping" of strands –as the spatial resolution of the thermal camera prevents capturing finer detail. Notice,

however, that the filament regularization step eliminates this artifact to some extent.

Because of the way data was captured –one 360 ° turn at constant height around the hairstyle– some regions are far from the center of projection (or not even visible). Points located at those regions cannot be faithfully reconstructed, since photo-consistency tends to be unstable in such cases, which can even lead to hairless spots due to the lack of boundary information. Similarly, for long hair, areas below the shoulders have not been captured during data acquisition. Please note, however, that this issue can be greatly reduced by including additional viewing angles. Finally, the shape of long or extremely voluminous hairstyles tends to be less constrained by the shape of the underlying head/body parts making both hair-skin temperature segmentation and feature extraction more challenging.

Despite limitations, we believe that our thermal based approach provides an alternative technique with which promising results can be obtained relative simple and easy. The results of our approach can be seen in Figure 3.21, where different views of the synthesized hair geometries have been visualized using a physically accurate rendering system, including shadowing and global illumination.

3.6 Conclusions

The advantages of using thermal data as input can be seen in almost every stage of our approach. Based on the temperature information we accomplish the segmentation of the hair region in a simple, relatively fast and robust way. Moreover, the use of accelerated photo-consistency allows for the reconstruction of complex hair shapes without any constraints regarding lighting, even from the lower resolution images provided by cost effective thermal video cameras. In the future we would like to explore methods that combine complementary strength of optical and thermal imaging to capture both high resolution shape and reflectance at the same time.

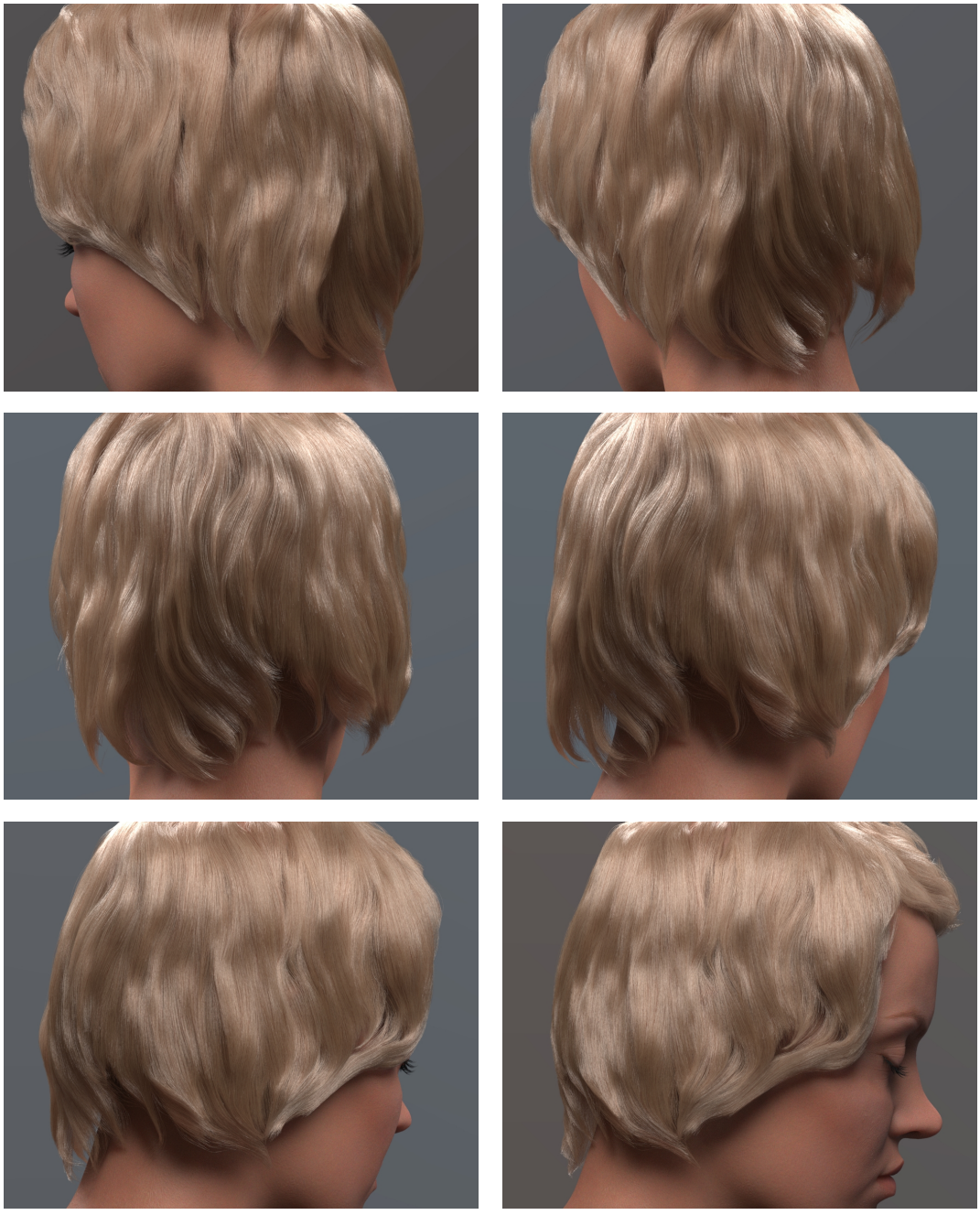

Figure 3.21: Final renderings of the reconstructed hairstyles.

4

Conclusions and Future Work

We have illustrated how facial hair can be easily transferred between different models following the approach described in chapter 2. Moreover, with the help of the database-driven prior the semblance of the facial hair from a shaven subject can be estimated. This can be very useful in fields like criminology, where the appearance of a bearded subject can be inferred from a shaven picture, combining our approach with the "Morphable Head Model" [PKA+09].

Enhancing the facial texture database with subjects of different races would increase the accuracy of our technique, since the generated prior would be more general. Moreover, it would be interesting to analyse the impact of different characterizations of the skin (and hair) pixels as well as different ways of computing the probability map along the facial texture image on the performance of our method.

As shown in chapter 3, the use of thermal imaging allow us to improve almost every step in the hairstyle reconstruction pipeline and to obtain results

comparable to other reconstruction approaches with a much more complex acquisition setup. The main advantages are

- Considerably simpler and faster data acquisition: No dedicated illumination, only a hand-held camera is required.
- Extremely simple and robust hair region segmentation: Our temperature-based segmentation technique outperforms all other proposed methods for the extraction of the hair region (done mostly manually).
- Accelerated surface reconstruction by means of temperature-based photo-consistency: The temperature distribution along the hairstyle surface, result of the heat emitted by the head and re-emitted by the hairs, help us to avoid illumination issues –like self-shadowing, directional reflectance, highlights– that have a negative impact in the reconstruction process.

Even more satisfactory results should be obtained if the thermal data can be combined with conventional image data, taking advantage of both types of information. The color of the hair filaments can be computed from the conventional images, giving thus more realism to the generated hair geometry. Moreover, the resolution of conventional cameras –currently at least one order of magnitude higher than the resolution of thermal cameras– allows to capture more detail from the modeled hair. Finally, the reflectance information of the hair fibers, obtained from conventional imaging and external light sources, gives even more information regarding the shape of the hairstyle.

Even if a local relationship can be established based on the monotony between the temperature at the hairstyle surface and its distance to the scalp, we have no information regarding the position (and shape) of the scalp except for some sparse spots in the thermal images where –according to the measured temperature– the scalp is visible. It would be interesting to investigate whether it is possible to estimate the shape and position of the scalp based on the body temperature –measured by capturing the face of the model– assuming that the scalp surface can be computed by solving a

boundary-value problem in which heat is emitted from an unknown surface at a constant rate and travels trough a homogeneous medium until it reaches the outermost boundary –the reconstructed hairstyle surface.

Bibliography

[AKN+11] Antonini, S. ; Kolaric, D. ; Nola, I.A. ; Herceg, Z. ; Ramljak, V. ; Kulis, T. ; Holjevac, J.K. ; Ferencic, Z.: Thermography surveillance after breast conserving surgery: Three cases. In: *ELMAR, 2011 Proceedings*, 2011. – ISSN 1334–2630, S. 317 –319 6

[AUK92] Anjyo, Ken-ichi ; Usami, Yoshiaki ; Kurihara, Tsuneya: A simple method for extracting the natural beauty of hair. In: *SIGGRAPH Comput. Graph.* 26 (1992), Juli, Nr. 2, 111–120. http://dx.doi.org/10.1145/142920.134021. – DOI 10.1145/142920.134021. – ISSN 0097–8930 7, 35, 40

[BAC+06] Bertails, Florence ; Audoly, Basile ; Cani, Marie-Paule ; Querleux, Bernard ; Leroy, Frédéric ; Lévêque, Jean-Luc: Super-helices for predicting the dynamics of natural hair. In: *ACM Trans. Graph.* 25 (2006), Juli, Nr. 3, 1180–1187. http://dx.doi.org/10.1145/1141911.1142012. – DOI 10.1145/1141911.1142012. – ISSN 0730–0301 64

[BAF07] Bauer, N. ; Angewandten Forschung, Fraunhofer-Gesellschaft zur Förderung der: *Handbuch zur industriellen Bildverarbeitung: Qualitätssicherung in der Praxis*. Fraunhofer-IRB-Verl., 2007 http://books.google.de/books?id=ZmBvhgYUg0AC. – ISBN 9783816773863 45

[BAQ+05] Bertails, Florence ; Audoly, Basile ; Querleux, Bernard

; Leroy, Frédéric ; Lévêque, Jean-Luc ; Cani, Marie-Paule: Predicting Natural Hair Shapes by Solving the Statics of Flexible Rods. In: Ganovelli F., Dingliana J. (Hrsg.): *Eurographics Short Papers*. Dublin, Ireland : Eurographics, 2005 7, 36, 41

[BBN+12] Beeler, Thabo ; Bickel, Bernd ; Noris, Gioacchino ; Beardsley, Paul ; Marschner, Steve ; Sumner, Robert W. ; Gross, Markus: Coupled 3D reconstruction of sparse facial hair and skin. In: *ACM Trans. Graph.* 31 (2012), Juli, Nr. 4, 117:1–117:10. http://dx.doi.org/10.1145/2185520.2185613. – DOI 10.1145/2185520.2185613. – ISSN 0730–0301 9

[BCN03] Bando, Yosuke ; Chen, Bing-Yu ; Nishita, Tomoyuki: Animating Hair with Loosely Connected Particles. In: *Computer Graphics Forum* 22 (2003), Nr. 3, 411–418. http://dx.doi.org/10.1111/1467-8659.00688. – DOI 10.1111/1467–8659.00688. – ISSN 1467–8659 7

[BHC+08] Bertails, Florence ; Hadap, Sunil ; Cani, Marie-Paule ; Lin, Ming ; Kim, Tae-Yong ; Marschner, Steve ; Ward, Kelly ; Kačić-Alesić, Zoran: Realistic hair simulation: animation and rendering. In: *ACM SIGGRAPH 2008 classes*. New York, NY, USA : ACM, 2008 (SIGGRAPH '08), 89:1–89:154 9, 35

[BK04] Boykov, Y. ; Kolmogorov, V.: An experimental comparison of min-cut/max- flow algorithms for energy minimization in vision. In: *Pattern Analysis and Machine Intelligence, IEEE Transactions on* 26 (2004), September, Nr. 9, S. 1124–1137. http://dx.doi.org/10.1109/TPAMI.2004.60. – DOI 10.1109/TPAMI.2004.60. – ISSN 0162–8828 27

[BR02] Bernardini, Fausto ; Rushmeier, Holly: The 3D Model Acquisition Pipeline. In: *Computer Graphics Forum* 21 (2002), Nr.

2, 149–172. http://dx.doi.org/10.1111/1467-8659.00574. – DOI 10.1111/1467–8659.00574. – ISSN 1467–8659 6

[Bro12] Brooks, Peter: *Testing Building Envelopes with Infrared Thermography; Delivering the "Big Picture"*, 2007 (accessed October 2, 2012). http://www.rci-online.org/interface/2007-07-brooks.pdf 6

[BT93] Bertsimas, Dimitris ; Tsitsiklis, John: Simulated Annealing. In: *Statistical Science* 8 (1993), Nr. 1, 10–15. http://dx.doi.org/10.1214/ss/1177011077. – DOI 10.1214/ss/1177011077. – ISBN 9789537619077 58

[BTL+11] Bilodeau, Guillaume-Alexandre ; Torabi, Atousa ; Lévesque, Maxime ; Ouellet, Charles ; Langlois, J. M. P. ; Lema, Pablo ; Carmant, Lionel: Body temperature estimation of a moving subject from thermographic images. In: *Machine Vision and Applications* 23 (2011), Januar, Nr. 2, 299–311. http://dx.doi.org/10.1007/s00138-010-0313-9. – DOI 10.1007/s00138–010–0313–9. – ISSN 0932–8092 6

[BV99] Blanz, Volker ; Vetter, Thomas: A morphable model for the synthesis of 3D faces. In: *Proceedings of the 26th annual conference on Computer graphics and interactive techniques*. New York, NY, USA : ACM Press/Addison-Wesley Publishing Co., 1999 (SIGGRAPH '99). – ISBN 0–201–48560–5, 187–194 29

[BV06] Boykov, Y. ; Veksler, O.: Graph Cuts in Vision and Graphics: Theories and Applications. In: Paragios, Nikos (Hrsg.) ; Chen, Yunmei (Hrsg.) ; Faugeras, Olivier (Hrsg.): *Handbook of Mathematical Models in Computer Vision*. New York : Springer US, 2006. – ISBN 0–387–26371–3, Kapitel 5, S. 79–96 13

[BWBM06] Brox, Thomas ; Weickert, Joachim ; Burgeth, Bernhard ; Mrázek, Pavel: Nonlinear structure tensors. In: *Im-*

age and Vision Computing 24 (2006), Januar, Nr. 1, 41–55. http://dx.doi.org/10.1016/j.imavis.2005.09.010. – DOI 10.1016/j.imavis.2005.09.010. – ISSN 02628856 16

[CIIP12] Cardone, Gennaro ; Ianiro, Andrea ; Ioio, Gennaro dello ; Passaro, Andrea: Temperature maps measurements on 3D surfaces with infrared thermography. In: *Experiments in Fluids* 52 (2012), November, Nr. 2, 375–385. http://dx.doi.org/10.1007/s00348-011-1225-9. – DOI 10.1007/s00348–011–1225–9. – ISBN 0034801112259 6

[CK05] Choe, Byoungwon ; Ko, Hyeong-Seok: A Statistical Wisp Model and Pseudophysical Approaches for Interactive Hairstyle Generation. In: *IEEE Transactions on Visualization and Computer Graphics* 11 (2005), März, Nr. 2, 160–170. http://dx.doi.org/10.1109/TVCG.2005.20. – DOI 10.1109/TVCG.2005.20. – ISSN 1077–2626 7, 36, 39, 40, 42

[CSDI99] Chen, Lieu-Hen ; Saeyor, Santi ; Dohi, Hiroshi ; Ishizuka, Mitsuru: A system of 3D hair style synthesis based on the wisp model. In: *The Visual Computer* 15 (1999), Juli, Nr. 4, 159–170. http://dx.doi.org/10.1007/s003710050169. – DOI 10.1007/s003710050169. – ISSN 01782789 39

[DB96] Dereniak, Eustace L. ; Boreman, G.D.: *Infrared detectors and systems*. Wiley, 1996 (Wiley series in pure and applied optics). – ISBN 9780471122098 45

[FA91] Freeman, W.T. ; Adelson, E.H.: The Design and Use of Steerable Filters. In: *IEEE Transactions on Pattern Analysis and Machine Intelligence* 13 (1991), S. 891–906. http://dx.doi.org/http://doi.ieeecomputersociety.org/10.1109/34.93808. – DOI http://doi.ieeecomputersociety.org/10.1109/34.93808. – ISSN 0162–8828 15, 16, 24

[FE08] Fechteler, Philipp ; Eisert, Peter: Adaptive color classification for structured light systems. In: *Computer Vision and Pattern Recognition Workshops, 2008. CVPRW '08. IEEE Computer Society Conference on*, IEEE, june 2008. – ISBN 978–1–4244–2339–2, 1–7 6

[Fil10] In: Bloch, Isabelle (Hrsg.) ; Cesar, Jr. Roberto M. Roberto M. (Hrsg.): *Progress in Pattern Recognition, Image Analysis, Computer Vision, and Applications* Bd. 6419. 2010. – ISBN 978–3–642–16686–0 6

[FM02] Feng, Xiaoguang ; Milanfar, Peyman: Multiscale principal components analysis for image local orientation estimation, 2002. – ISBN 0780375769, 478–482 15

[Fre92] Freeman, William T.: *Steerable filters and local analysis of image structure*, Diss., 1992. http://citeseerx.ist.psu.edu/viewdoc/download?doi=10.1.1.33.2782 24, 59

[FW06] Fleet, David ; Weiss, Yair: Optical Flow Estimation. In: Paragios, Nikos (Hrsg.) ; Chen, Yunmei (Hrsg.): *Handbook of Mathematical Models in Computer Vision*. Springer, 2006. – ISBN 0–387–26371–6, Kapitel 15 70

[FWTQ07] Fu, Hongbo ; Wei, Yichen ; Tai, Chiew-Lan ; Quan, Long: Sketching hairstyles. In: *Proceedings of the 4th Eurographics workshop on Sketch-based interfaces and modeling*. New York, NY, USA : ACM, 2007 (SBIM '07). – ISBN 978–1–59593–915–9, 31–36 41

[GAVN11] Gupta, Mohit ; Agrawal, Amit ; Veeraraghavan, Ashok ; Narasimhan, Srinivasa G.: Structured light 3D scanning in the presence of global illumination. In: *Computer Vision and Pattern Recognition (CVPR), 2011 IEEE Conference on*, IEEE, june 2011. – ISBN 978–1–4577–0394–2, 713–720 6

[GS06] Gasparini, Francesca ; Schettini, Raimondo: Skin segmentation using multiple thresholding. In: *Proceedings of SPIE* (2006), 60610F-60610F-8. http://dx.doi.org/10.1117/12.647446. – DOI 10.1117/12.647446 14

[GSML02] Grabli, Stéphane ; Sillion, François X. ; Marschner, Stephen R. ; Lengyel, Jerome E.: Image-Based Hair Capture by Inverse Lighting. In: *Proceedings of Graphics Interface (GI)*. Calgary, Alberta, Canada, 2002, 51–58 8, 42

[HCL+07] Hadap, Sunil ; Cani, Marie-Paule ; Lin, Ming ; Kim, Tae-Yong ; Bertails, Florence ; Marschner, Steve ; Ward, Kelly ; Kačić-Alesić, Zoran: Strands and hair: modeling, animation, and rendering. In: *ACM SIGGRAPH 2007 courses*. New York, NY, USA : ACM, 2007 (SIGGRAPH '07). – ISBN 978–1–4503–1823–5, 1–150 9, 35

[HMT00] Hadap, S. ; Magnenat-Thalmann, N.: Interactive Hair Styler based on Fluid Flow. In: *Eurographics Workshop on Computer Animation and Simulation 2000*, Springer, August 2000, S. 87–99 7, 36, 41

[HZ04] Hartley, Richard ; Zisserman, Andrew: *Multiple View Geometry in Computer Vision*. Cambridge University Press, 2004 http://books.google.de/books?id=si3R3Pfa98QC. – ISBN 9780521540513 6

[JMM09] Jakob, Wenzel ; Moon, Jonathan T. ; Marschner, Steve: Capturing hair assemblies fiber by fiber. In: *ACM SIGGRAPH Asia 2009 papers*. New York, NY, USA : ACM, 2009 (SIGGRAPH Asia '09). – ISBN 978–1–60558–858–2, 164:1–164:9 8, 36, 43

[JR99] Jones, Michael J. ; Rehg, James M.: Statistical color models with application to skin detection. In: *International Journal of*

Computer Vision, IEEE Comput. Soc, 1999. – ISBN 0–7695–0149–4, S. 274–280 14

[KHSB12] Khan, Rehanullah ; Hanbury, Allan ; Stöttinger, Julian ; Bais, Abdul: Color based skin classification. In: *Pattern Recognition Letters* 33 (2012), Januar, Nr. 2, 157–163. http://dx.doi.org/10.1016/j.patrec.2011.09.032. – DOI 10.1016/j.patrec.2011.09.032. – ISSN 01678655 14

[KMB07] Kakumanu, P ; Makrogiannis, S ; Bourbakis, N: A survey of skin-color modeling and detection methods. In: *Pattern Recognition* 40 (2007), Nr. 3, 1106–1122. http://dx.doi.org/10.1016/j.patcog.2006.06.010. – DOI 10.1016/j.patcog.2006.06.010 14, 17

[KN98] Kong, Waiming ; Nakajima, Masayuki: Generation of 3D Hair Model from Multiple Pictures. In: *The Journal of the Institute of Image Information and Television Engineers* 52 (1998), Nr. 9, S. 1351–1356. http://dx.doi.org/10.3169/itej.52.1351. – DOI 10.3169/itej.52.1351. – ISSN 1881–6908 42

[KN00] Kim, Tae-Yong ; Neumann, U.: A thin shell volume for modeling human hair. In: *Computer Animation 2000. Proceedings*, 2000. – ISSN 1087–4844, S. 104 –111 7, 36, 39

[KN02] Kim, Tae-Yong ; Neumann, Ulrich: Interactive multiresolution hair modeling and editing. (2002), 620–629. http://dx.doi.org/10.1145/566570.566627. – DOI 10.1145/566570.566627. ISBN 1–58113–521–1 7, 36, 40

[Kot03] Kothe, U: Integrated edge and junction detection with the boundary tensor. In: *Proceedings Ninth IEEE International Conference on Computer Vision*, IEEE, 2003. – ISBN 0–7695–1950–4, 424–431 vol.1 16

[KPS03] Kovac, J. ; Peer, P. ; Solina, F.: Human skin color clustering for face detection. In: *EUROCON 2003. Computer as a Tool. The IEEE Region 8* Bd. 2, 2003, S. 144 – 148 vol.2 14

[LAGJ+12] Lagüela, S ; Armesto, J ; Gonzalez-Jorge, H ; Arias, P ; Herraez, P: Automation of thermographic 3D modelling through image fusion and image matching techniques. In: *Automation in Construction* 27 (2012), 24–31. http://dx.doi.org/10.1016/j.autcon.2012.05.011. – DOI 10.1016/j.autcon.2012.05.011. – ISSN 0926–5805 7

[LASG08] Lee, Kuang chih ; Anguelov, D. ; Sumengen, B. ; Gokturk, S.B.: Markov random field models for hair and face segmentation, 2008. – ISBN 9781424421541, 1–6 15

[Lau94] Laurentini, A: The visual hull concept for silhouette-based image understanding. In: *Pattern Analysis and Machine Intelligence, IEEE Transactions on* 16 (1994), feb, Nr. 2, 150 -162. http://dx.doi.org/10.1109/34.273735. – DOI 10.1109/34.273735. – ISSN 0162–8828 52

[LH03] Liang, Wenqi ; Huang, Zhiyong: An Enhanced Framework for Real-Time Hair Animation. In: *Proceedings of the 11th Pacific Conference on Computer Graphics and Applications*. Washington, DC, USA : IEEE Computer Society, 2003 (PG '03). – ISBN 0–7695–2028–6, 467– 39

[Llo06] Lloyd, S.: Least squares quantization in PCM. In: *IEEE Trans. Inf. Theor.* 28 (2006), September, Nr. 2, 129–137. http://dx.doi.org/10.1109/TIT.1982.1056489. – DOI 10.1109/TIT.1982.1056489. – ISSN 0018–9448 13

[LOPR10] Luhmann, Thomas ; Ohm, Julia ; Piechel, Johannes ; Roelfs, Thorsten: Geometric calibration of thermographic cameras. In: *International Archives of Photogrammetry, Re-*

mote Sensing and Spatial Information Sciences Bd. 38, 2010, 410–416 7

[LS83] Low, M. J. D. ; Severdia, A. G.: Infrared Spectra of a Single Human Hair. In: *Spectroscopy Letters* 16 (1983), November, Nr. 11, 871–877. http://dx.doi.org/10.1080/00387018308062396. – DOI 10.1080/00387018308062396. – ISSN 0038–7010 47

[MB98] Martinez, Aleix ; Benavente, Robert: The AR face database. In: *CVC Technical Report* 24 (1998). http://ci.nii.ac.jp/naid/10012519345/en/ 15

[Mer12] Merchant, John: *Infrared Temperature Measurement Theory and Application*, accessed October 2, 2012. http://www.omega.com/techref/iredtempmeasur.html 6

[MS89] Mumford, David ; Shah, Jayant: Optimal approximations by piecewise smooth functions and associated variational problems. In: *Communications on Pure and Applied Mathematics* 42 (1989), Nr. 5, S. 577–685. http://dx.doi.org/10.1002/cpa.3160420503. – DOI 10.1002/cpa.3160420503. – ISSN 1097–0312 13

[MS98] Malladi, R. ; Sethian, J.A.: A real-time algorithm for medical shape recovery. In: *Computer Vision, 1998. Sixth International Conference on*, 1998, S. 304 –310 50

[MSV95] Malladi, R. ; Sethian, J.a. ; Vemuri, B.C.: Shape modeling with front propagation: a level set approach. In: *IEEE Transactions on Pattern Analysis and Machine Intelligence* 17 (1995), Nr. 2, 158–175. http://dx.doi.org/10.1109/34.368173. – DOI 10.1109/34.368173. – ISSN 01628828 13

[MZ07] Mohr, Daniel ; Zachmann, Gabriel: Segmentation of distinct homogeneous color regions in images. In: *Proceedings of the 12th*

international conference on Computer analysis of images and patterns. Berlin, Heidelberg : Springer-Verlag, 2007 (CAIP'07). – ISBN 978–3–540–74271–5, 432–440 14

[Nol07] Nolting, J: Detektoren für optische Strahlung. In: *DOZ Optometrie* 4 (2007), 50–56. http://www.htw-aalen.de/dynamic/img/content/studium/a/publikationen/doz/2007/04_07_detektorenfueroptischestrahlen.pdf 45

[NT04] Noble, Paul ; Tang, Wen: Modelling and Animating Cartoon Hair with NURBS Surfaces. In: *Proceedings of the Computer Graphics International*. Washington, DC, USA : IEEE Computer Society, 2004 (CGI '04). – ISBN 0–7695–2171–1, 60–67 39

[PBC03] Phung, S.L. ; Bouzerdoum, Abdesselam ; Chai, Douglas: Skin segmentation using color and edge information. In: *Signal Processing and Its Applications, 2003. Proceedings. Seventh International Symposium on* Bd. 1, 2003, S. 525 – 528 vol.1 15

[PBC05] Phung, S.L. ; Bouzerdoum, Sr. A. ; Chai, Sr. D.: Skin segmentation using color pixel classification: analysis and comparison. In: *Pattern Analysis and Machine Intelligence, IEEE Transactions on* 27 (2005), jan., Nr. 1, S. 148 – 154. http://dx.doi.org/10.1109/TPAMI.2005.17. – DOI 10.1109/TPAMI.2005.17. – ISSN 0162–8828 14

[PBL04] Patrick, Deborah ; Bangay, Shaun ; Lobb, Adele: Modelling and rendering techniques for African hairstyles. In: *Proceedings of the 3rd international conference on Computer graphics, virtual reality, visualisation and interaction in Africa*. New York, NY, USA : ACM, 2004 (AFRIGRAPH '04). – ISBN 1–58113–863–6, 115–124 39, 40

[PBnS04] Paris, Sylvain ; Briceño, Hector M. ; Sillion, François X.: Capture of hair geometry from multiple images. In: *ACM SIG-*

GRAPH 2004 Papers. New York, NY, USA : ACM, 2004 (SIGGRAPH '04), 712–719 8, 24, 36, 42, 43, 44, 62

[PCK+08] Paris, Sylvain ; Chang, Will ; Kozhushnyan, Oleg I. ; Jarosz, Wojciech ; Matusik, Wojciech ; Zwicker, Matthias ; Durand, Frédo: Hair photobooth: geometric and photometric acquisition of real hairstyles. In: *ACM SIGGRAPH 2008 papers*. New York, NY, USA : ACM, 2008 (SIGGRAPH '08). – ISBN 978–1–4503–0112–1, 30:1–30:9 8, 36, 43, 62

[PKA+09] Paysan, Pascal ; Knothe, Reinhard ; Amberg, Brian ; Romdhani, Sami ; Vetter, Thomas: A 3D Face Model for Pose and Illumination Invariant Face Recognition. In: *AVSS '09: Proceedings of the 2009 Sixth IEEE International Conference on Advanced Video and Signal Based Surveillance*. Washington, DC, USA : IEEE Computer Society, 2009. – ISBN 978–0–7695–3718–4, S. 296–301 2, 6, 10, 25, 77

[Pow64] Powell, M. J. D.: An efficient method for finding the minimum of a function of several variables without calculating derivatives. In: *The Computer Journal* 7 (1964), Nr. 2, 155-162. http://dx.doi.org/10.1093/comjnl/7.2.155. – DOI 10.1093/comjnl/7.2.155 65

[Poy97] Poynton, Charles: *Frequently asked questions about color*. http://www.poynton.com/PDFs/ColorFAQ.pdf. Version: 1997 14

[PRO+02] Preciado, Jessica A. ; Rubinsky, Boris ; Otten, David ; Nelson, Brent ; Martin, Michael C. ; Greif, Ralph: Radiative Properties of Polar Bear Hair. In: *Proceedings of the ASME International Mechanical Engineering Congress and Exposition, November 17-22, 2002, New Orleans, Louisiana* Bd. BED-Vol. 53, ASME, 2002. – LBNL-50430, 1.4.3 47

[RC08] Rousset, C. ; Coulon, P.Y.: Frequential and color analysis for hair mask segmentation. In: *Image Processing, 2008. ICIP 2008. 15th IEEE International Conference on*, 2008. – ISSN 1522–4880, S. 2276 –2279 15

[Rob02] *Kapitel* Morphological and Macromolecular Structure. In: Robbins, Clarence R.: *Chemical and Physical Behavior of Human Hair*. Fourth Edition. Springer-Verlag New York, Inc, 2002 4

[Rob12] Roberts, Will: *How does thermal imaging work? A closer look at what is behind this remarkable technology*, 2007 (accessed October 2, 2012). http://www.video-surveillance-guide.com/how-does-thermal-imaging-work.htm 6

[SD97] Seitz, Steven M. ; Dyer, Charles R.: Photorealistic Scene Reconstruction by Voxel Coloring. In: *Proceedings of the 1997 Conference on Computer Vision and Pattern Recognition (CVPR '97)*. Washington, DC, USA : IEEE Computer Society, 1997 (CVPR '97). – ISBN 0–8186–7822–4, 1067– 52

[SF96] Simoncelli, E.P. ; Farid, H.: Steerable wedge filters for local orientation analysis. In: *Image Processing, IEEE Transactions on* 5 (1996), sep, Nr. 9, S. 1377 –1382. http://dx.doi.org/10.1109/83.535851. – DOI 10.1109/83.535851. – ISSN 1057–7149 15

[SH] Stennett, Carl ; Harris, Chris: 3D Computer Vision Techniques Applied to Infra-red Imagery 7

[SKW06] Sobottka, Gerrit ; Kusak, Michael ; Weber, Andreas: Hairstyle Construction from Raw Surface Data. In: *International Conference on Computer Graphics, Imaging and Visualisation (CGIV'06)*. Sydney, Australia : IEEE Computer Society, 2006. – ISBN 0–7695–2606–3, S. 365–371 7, 36, 41

[SLFW02] Sund-Levander, Mrtha ; Forsberg, Christina ; Wahren, Lis K.: Normal oral, rectal, tympanic and axillary body temperature in adult men and women: a systematic literature review. In: *Scandinavian Journal of Caring Sciences* 16 (2002), Nr. 2, 122–128. http://dx.doi.org/10.1046/j.1471-6712.2002.00069.x. – DOI 10.1046/j.1471–6712.2002.00069.x. – ISSN 1471–6712 46, 50

[SSS08] Snavely, Noah ; Seitz, Steven M. ; Szeliski, Richard: Modeling the World from Internet Photo Collections. In: *Int. J. Comput. Vision* 80 (2008), November, Nr. 2, 189–210. http://dx.doi.org/10.1007/s11263-007-0107-3. – DOI 10.1007/s11263–007–0107–3. – ISSN 0920–5691 49, 50

[Sun10] Sun, Hung-Ming: Skin detection for single images using dynamic skin color modeling. In: *Pattern Recogn.* 43 (2010), April, Nr. 4, 1413–1420. http://dx.doi.org/10.1016/j.patcog.2009.09.022. – DOI 10.1016/j.patcog.2009.09.022. – ISSN 0031–3203 14

[SV04] Solar, Javier Ruiz-del ; Verschae, Rodrigo: Skin detection using neighborhood information. In: *Proceedings of the Sixth IEEE international conference on Automatic face and gesture recognition*. Washington, DC, USA : IEEE Computer Society, 2004 (FGR' 04). – ISBN 0–7695–2122–3, 463–468 15

[THM+03] Teschner, Matthias ; Heidelberger, Bruno ; Mueller, Matthias ; Pomeranets, Danat ; Gross, Markus: Optimized Spatial Hashing for Collision Detection of Deformable Objects. In: *Proc. Vision, Modeling, Visualization (VMV'03)*. Munich, Germany, Nov 2003, 47–54 28

[TMHF00] Triggs, Bill ; McLauchlan, Philip F. ; Hartley, Richard I. ; Fitzgibbon, Andrew W.: Bundle Adjustment – A Modern Synthesis. In: *Proceedings of the International Workshop on*

Vision Algorithms: Theory and Practice. London, UK, UK : Springer-Verlag, 2000 (ICCV '99). – ISBN 3–540–67973–1, 298–372 49

[VHETC07] Vogiatzis, George ; Hernández Esteban, Carlos ; Torr, Philip H. S. ; Cipolla, Roberto: Multiview Stereo via Volumetric Graph-Cuts and Occlusion Robust Photo-Consistency. In: *IEEE Trans. Pattern Anal. Mach. Intell.* 29 (2007), Dezember, Nr. 12, 2241–2246. http://dx.doi.org/10.1109/TPAMI.2007.70712. – DOI 10.1109/TPAMI.2007.70712. – ISSN 0162–8828 53, 70

[VSA03] Vezhnevets, Vladimir ; Sazonov, Vassili ; Andreeva, Alla: A survey on pixel-based skin color detection techniques. In: *Proceedings of the GraphiCon 2003* Bd. 85, 2003, 85–92 14

[WBC07] Wither, Jamie ; Bertails, Florence ; Cani, Marie-Paule: Realistic Hair from a Sketch. In: *Shape Modeling International*, 2007 41

[WBK+07] Ward, Kelly ; Bertails, Florence ; Kim, Tae-Yong ; Marschner, Stephen R. ; Cani, Marie-Paule ; Lin, Ming C.: A Survey on Hair Modeling: Styling, Simulation, and Rendering. In: *IEEE Transactions on Visualization and Computer Graphics* 13 (2007), März, Nr. 2, 213–234. http://dx.doi.org/10.1109/TVCG.2007.30. – DOI 10.1109/TVCG.2007.30. – ISSN 1077–2626 9, 35, 38

[WLL+03] Ward, Kelly ; Lin, Ming C. ; Lee, Joohi ; Fisher, Susan ; Macri, Dean: Modeling Hair Using Level-of-Detail Representations. In: *Proceedings of the 16th International Conference on Computer Animation and Social Agents (CASA 2003)*. Washington, DC, USA : IEEE Computer Society, 2003 (CASA '03). – ISBN 0–7695–1934–2, 41– 7, 36, 40

[WOQS05] Wei, Yichen ; Ofek, Eyal ; Quan, Long ; Shum, Heung-Yeung: Modeling hair from multiple views. In: *ACM SIGGRAPH 2005 Papers*. New York, NY, USA : ACM, 2005 (SIGGRAPH '05), 816–820 8, 36, 43, 44, 60, 62

[WS92] Watanabe, Yasuhiko ; Suenaga, Yasuhito: A Trigonal Prism-Based Method for Hair Image Generation. In: *IEEE Comput. Graph. Appl.* 12 (1992), Januar, Nr. 1, 47–53. http://dx.doi.org/10.1109/38.135883. – DOI 10.1109/38.135883. – ISSN 0272–1716 7, 38

[WYZG09] Wang, Lvdi ; Yu, Yizhou ; Zhou, Kun ; Guo, Baining: Example-based hair geometry synthesis. In: *ACM SIGGRAPH 2009 papers*. New York, NY, USA : ACM, 2009 (SIGGRAPH '09). – ISBN 978–1–60558–726–4, 56:1–56:9 44, 62

[WZ85] Wolfe, William L. ; Zissis, George J.: *The Infrared handbook*. Environmental Research Institute of Michigan, 1985 (Press Monographs). http://books.google.de/books?id=LDhSAAAAMAAJ 46

[XY01] Xu, Zhan ; Yang, Xue D.: V-HairStudio: an interactive tool for hair design. In: *Computer Graphics and Applications, IEEE* 21 (2001), may/jun, Nr. 3, S. 36 –43. http://dx.doi.org/10.1109/38.920625. – DOI 10.1109/38.920625. – ISSN 0272–1716 39

[YC11] Yang, Rongqian ; Chen, Yazhu: Design of a 3-D Infrared Imaging System Using Structured Light. In: *Instrumentation and Measurement, IEEE Transactions on* 60 (2011), feb., Nr. 2, S. 608 –617. http://dx.doi.org/10.1109/TIM.2010.2051614. – DOI 10.1109/TIM.2010.2051614. – ISSN 0018–9456 6

[YD06] Yacoob, Yaser ; Davis, Larry S.: Detection and Analysis of Hair. In: *IEEE Trans. Pattern Anal. Mach. Intell.* 28 (2006),

July, 1164–1169. http://dx.doi.org/10.1109/TPAMI.2006.139. – DOI 10.1109/TPAMI.2006.139. – ISSN 0162–8828 15

[YSK09] Yuksel, Cem ; Schaefer, Scott ; Keyser, John: Hair meshes. In: *ACM SIGGRAPH Asia 2009 papers*. New York, NY, USA : ACM, 2009 (SIGGRAPH Asia '09). – ISBN 978–1–60558–858–2, 166:1–166:7 7, 36, 39

[Yu01] Yu, Yizhou: Modeling Realistic Virtual Hairstyles. In: *Proceedings of the 9th Pacific Conference on Computer Graphics and Applications*. Washington, DC, USA : IEEE Computer Society, 2001 (PG '01). – ISBN 0–7695–1227–5, 295– 41

[ZRL+09] Zinke, Arno ; Rump, Martin ; Lay, Tomás ; Weber, Andreas ; Andriyenko, Anton ; Klein, Reinhard: A practical approach for photometric acquisition of hair color. In: *ACM SIGGRAPH Asia 2009 papers*. New York, NY, USA : ACM, 2009 (SIGGRAPH Asia '09). – ISBN 978–1–60558–858–2, 165:1–165:9 31

[ZW07] Zinke, Arno ; Weber, Andreas: Light Scattering from Filaments. In: *IEEE Transactions on Visualization and Computer Graphics* 13 (2007), März, Nr. 2, 342–356. http://dx.doi.org/10.1109/TVCG.2007.43. – DOI 10.1109/TVCG.2007.43. – ISSN 1077–2626 29, 31